Published by
NIGERIAN SOCIETY OF PHYSICAL SCIENCES
Available online @ https://journal.nsps.org.ng/index.php/jnsps

J. Nig. Soc. Phys. Sci. 8 (2026) 3254

Journal of the Nigerian Society of Physical Sciences

Privacy-preserving visual analytics using complex single-valued neutrosophic sets and encrypted dimensionality reduction

Raed Hatamleh[a], Abdallah Shihadeh[b], Wael Mahmoud Mohammad Salameh[c], Aqeedat Hussain[d], Arif Mehmood[d], Walid Abdelfattah[e,*], Jamil J. Hamja[f], Cris L. Armada[g,h]

[a]*Department of Mathematics, Faculty of Science, Jadara University, P.O. Box 733, Irbid 21110, Jordan*
[b]*Department of Mathematics, Faculty of Science, The Hashemite University, Zarqa 13133, P.O. Box 330127, Jordan*
[c]*Faculty of Information Technology, Abu Dhabi University, Abu Dhabi, United Arab Emirates*
[d]*Department of Mathematics, Institute of Numerical Sciences, Gomal University, Dera Ismail Khan 29050, KPK, Pakistan*
[e]*Humanities and Social Research Center, Northern Border University, Arar, Saudi Arabia*
[f]*Department of Mathematics, College of Mathematical Sciences, Mindanao State University Tawi-Tawi College of Technology and Oceanography, Philippines*
[g]*Vietnam National University Ho Chi Minh City, Linh Trung Ward, Thu Duc City, Ho Chi Minh City, Vietnam*
[h]*Department of Applied Mathematics, Faculty of Applied Science, Ho Chi Minh City University of Technology (HCMUT), 268 Ly Thuong Kiet, Ward 14, District 10, Ho Chi Minh City, Vietnam*

Abstract

This article introduces a new concept of complex single-valued neutrosophic sets (CSVNS) and explores their basic set-theoretic characteristics. Based on this framework, an approach to visual analytics that preserves privacy for high-dimensional data, but remains fully encrypted, is proposed. The proposed scheme shows how information about the similarity of the cotangents of functions can be encrypted while retaining its fundamental analytical properties. Three-dimensional (3D) encrypted parallel coordinates visualizations, 3D t-distributed stochastic neighbor embedding (t-SNE) visualizations, and encrypted Pearson correlation heatmaps accurately capture the similarity patterns of the original data while introducing only controlled and minor perturbations to the best matching pairs, variance distribution, class relationships, and correlation structures. The small differences in variance and normalized similarity values show that the encryption mechanism had little effect on the data, which means that the geometric and relational features of the dataset are suitable for analysis in the encrypted domain. The proposed approach is a powerful solution for secure similarity analysis, dimensionality reduction, clustering, and privacy-preserving decision support applications, while retaining analytical accuracy.

DOI: 10.46481/jnsps.2026.3254

Keywords: Neutrosophic set, Single-valued neutrosophic set, Complex single-valued neutrosophic set, Privacy-preserving encryption, Cotangent similarity measure

Article History:
Received: 02 January 2026
Received in revised form: 25 June 2026
Accepted for publication: 07 July 2026
Available online: 24 August 2026

Communicated by: B. J. Falaye

1. Introduction

Zadeh [1] was the first to establish the idea of fuzzy sets, which altered the field of mathematical modeling and control theory by modeling the imprecision and uncertainty present in real-world problems. Later, Chang and Zadeh [2] expanded this

*Corresponding Author Tel. No.: +966-549-438-036.
Email address: walid.abdelfattah@nbu.edu.sa (Walid Abdelfattah)

work to fuzzy mapping and control, and Dubois and Prade [3] expanded it to crucial operations on fuzzy numbers, resulting in a potent framework for handling ambiguous data. Atanassov [4] made a significant generalization by introducing intuitionistic fuzzy sets (IFSs), which used a non-membership degree to provide a more nuanced representation of uncertainty with membership and non-membership degrees adding up to a total less than or equal to one.

The three separate components of fuzzy and intuitionistic fuzzy sets truth-membership (T), indeterminacy-membership (I), and falsity-membership (F) were then presented by Smarandache [5, 6] as neutrosophic sets (NSs). Classical fuzzy logic cannot handle ambiguous and inconsistent information; only this three-part approach can. By developing different kinds of triangular neutrosophic numbers and de-neutrosophication techniques, Chakraborty *et al.* [7] advanced the science and increased the viability of NSs in quantitative applications. Neutrosophic uses proliferated during the following decade, particularly in multi-criteria decision-making (MCDM).

For example, Abdel-Basset *et al.* [8] proposed a hybrid NS-based group decision-making framework for project selection, while Ojo *et al.* [9] examined green supply chain management practices and Abdel-Baset *et al.* [10] studied sustainable supplier selection using a neutrosophic framework. By using methods like TOPSIS and DEMATEL, Abdel-Basset *et al.*'s additional works [11]-[12] extended neutrosophic MCDM to resource leveling, medical equipment selection, and supplier selection. Abdel-Basset *et al.* [13] created a bipolar neutrosophic professional selection, whereas Saqlain *et al.* [14] suggested a neutrosophic soft set of generalized fuzzy TOPSIS to choose smartphones. More recently, Riaz and Farid [15] maximized green supply chain efficiency using linear Diophantine fuzzy aggregation operators, while Abdel-Basset and Mohamed [16] suggested a plithogenic TOPSIS-CRITIC model of supply chain risk management.

Smarandache [17] continued to refine the theoretical underpinnings of neutrosophic logic concurrently. Significant advancements in MCDM techniques have coincided with these developments in uncertainty modeling. A summary of the TOPSIS technique, one of the most widely used MCDM techniques, was provided by Zavadskas *et al.* [18]. Garg and Kumar [19] created the similarity measures of IFSs using set pair analysis, whereas Peng and Dai [20] evaluated the quality of classroom instruction using q-rung orthopair fuzzy information. The Pythagorean Dombi fuzzy aggregation operators of MCDM, which demonstrate the ongoing evolution of fuzzy systems, were created by Akram *et al.* [21]. In a distinct but equally significant area, steganography and cryptography have contributed to secure communication.

1.1. Literature review

The Advanced Encryption Standard (AES) and broad introductions to cryptography are found in textbooks by Delfs and Knebl [22] and Daemen and Rijmen [23], respectively. Philip [24] proposed an extended pseudo-knight tour algorithm that could be used to encrypt images, while Al-Assam *et al.* [25] coupled steganography with biometric cryptosystems to provide safe two-way authentication. Steganography and cryptography on images were studied by Bloisi and Iocchi [26] and Sharma [27]. Based on computer-generated holograms and chaos theory, the optical color picture encryption described by Liu *et al.* [28] was created using Shannon's secrecy systems communication theory [29]. A didactic example of chocolate key cryptography was presented by Bachman *et al.* [30].

Rosenthal [31] described Rijndael in polynomial form, Koc [32] talked about cryptographic engineering, Liu *et al.* [33] looked at the complexity of AES S-boxes, and AES algebraic structure has been well studied. Steganography and cryptography can be combined to enhance information security by providing multiple layers of protection for sensitive data. The integration of these techniques can improve confidentiality and reduce the risk of unauthorized access or detection of hidden information, as discussed by Challita and Farhat [34]. Algebraic representations of Rijndael were covered by Ferguson *et al.* [35] and Murphy and Robshaw [36], while various S-box modifications intended to enhance cryptographic features were described by Cui and Cao [37], Li *et al.* [38], Khan and Azam [39, 40], and Tran *et al.* [41]. The unifying field of neutrosophic logic and probability was still being worked on by Smarandache [42]. These two fields have converged in recent years, and fuzzy and neutrosophic models are being applied more frequently to solve challenging analytical issues. A. Ahmad *et al.* [43] suggested k-threshold conversion number in neutrosophic graphs. On the numerical solutions for some neutrosophic singular boundary value problems by using (LPM) polynomials were studied by A. A. Abubaker *et al.* [44].

Hatamleh and Hazaymeh [45] studied plithogenic interval-based topological spaces, while Hatamleh *et al.* [46] suggested intricate tangent trigonometric techniques to create fuzzy sets. The fixed point results in metric spaces and fuzzy b-metric spaces were developed by Qawaqneh [47] and Qawaqneh *et al.* [48, 49]. Fractional soliton solutions and fixed-point functions were studied by Qawaqneh *et al.* [50] and [51], whereas contraction mappings in fractional metric spaces were studied by Qawaqneh *et al.* [52]. Raed Hatamleh and Ayman Hazaymeh [53] gave the concept for finding minimal units in several two-fold fuzzy finite neutrosophic rings. The Internet of Things (IoT) has the potential to transform education by enabling smart learning environments, personalized learning experiences, and improved interaction between teachers and students. IoT-enabled devices can support customized learning and enhance collaboration, although challenges such as privacy, cybersecurity, and technical expertise remain significant concerns (Kanan *et al.*) [54]. Fractional-order PID controllers were modeled in robot arm models by Batiha *et al.* [55]. Soft set theory's theoretical underpinnings have also seen significant development.

New kinds of supra soft continuous maps were proposed by Abd El-latif and Alqahtani [56], and a larger set of soft sets with supra soft δ-closure operators was proposed by Abd El-latif *et al.* [57]. Abd El-latif *et al.* [58, 59] provided new versions of maps and applications of soft anywhere dense sets, while

Al-Omari and Alqahtani [60] investigated the operators in soft primal spaces. Alqahtani [61] defined operators and separation axioms in diving topological spaces, whereas Alqahtani [62] proposed neutrosophic primal structures, closure, and proximity operators. Alqahtani and Tkachenko [63] investigated normality in topological groups, while Ibedou *et al.* [64] presented new structures on universal sets. El-Sheikh and Abd El-latif broke down supra soft sets and soft continuity [65] and also presented specific types of Lindelofness and compactness based on novel supra soft operator [66], whereas Abd El-latif and Alqahtani [67, 68] created new soft operators, separation axioms, and their applications.

1.2. Research gap

Only low-dimensional complex single-valued neutrosophic sets (CSVNSs) have been studied theoretically. It is evident that there is a lack of integration between CSVNS theory and existing visual analytics techniques for handling high-dimensional data. Furthermore, the visual study of fully encrypted material to preserve the structural linkages is lacking in the existing frameworks. Furthermore, up until now, uncertainty modeling, encryption, dimensionality reduction, and visualization have not all been taken into account in a single analytical framework.

1.3. Novelty

The paper offers a single paradigm that integrates encrypted visual analytics with multifaceted single-valued neutrosophic set theory. To preserve neighborhood relationships and class hierarchy without granting access to underlying numerical data, it employs t-distributed stochastic neighbor embedding (t-SNE), an encrypted three-dimensional representation. To make the visualizations easier to understand, parallel coordinates, a heatmap of correlation, and a 3D scatter plot are used for normalization and encryption. In order to support the effectiveness of the proposed approach in the context of secure data analysis, the results demonstrate that fundamental geometric, topological, and relational structures may still be understood in their encrypted form.

2. Preliminaries

In this section, we will give some preliminary information for the present study.

Definition 2.1. *[5, 42] Let $\mathcal{U}$ be an universe of discourse. Then the neutrosophic set* P *can be presented of the form:*

$$\mathrm{P} = \{\langle \mathbf{x}, \mathrm{T}_P(\mathbf{x}), \mathrm{I}_P(\mathbf{x}), \mathrm{F}_P(\mathbf{x})\rangle : \mathbf{x} \in \mathcal{U}\}$$

where the function $\mathrm{T}, \mathrm{I}, \mathrm{F} : U \longrightarrow]^{-}0,^{+}1[$ *defines respectively the degree of membership, the degree of indeterminacy, and the degree of non-membership of the element* $\mathbf{x} \in \mathcal{U}$ *to the set* P *satisfying the following condition.*

$$^{-}0 \le sup\mathrm{T}_P(\mathbf{x}) + sup\mathrm{I}_P(\mathbf{x}) + sup\mathrm{F}_P(\mathbf{x}) \le 3^{+}$$

From philosophical point of view, the neutrosophic set assumes the value from real standard or non-standard subsets of $]^{-}0,^{+}1[$. *So instead of* $]^{-}0,^{+}1[$ *needs to take the interval* $[0,1]$ *for technical applications, because* $]^{-}0,^{+}1[$ *will be difficult to apply in the real applications such as scientific and engineering problems.*

Definition 2.2. *[5, 42] Let there be two neutrosophic sets (NSs),*

$$P_{NS} = \{\langle \mathbf{x}, \mathrm{T}_P(\mathbf{x}), \mathrm{I}_P(\mathbf{x}), \mathrm{F}_P(\mathbf{x})\rangle : \mathbf{x} \in \mathbb{X}\}$$

and

$$Q_{NS} = \{\langle \mathbf{x}, \mathrm{T}_Q(\mathbf{x}), \mathrm{I}_Q(\mathbf{x}), \mathrm{F}_Q(\mathbf{x})\rangle : \mathbf{x} \in \mathbb{X}\}$$

then $P_{NS} \subseteq Q_{NS}$ *iff* $\mathrm{T}_P(\mathbf{x}) \le \mathrm{T}_Q(\mathbf{x}), \mathrm{I}_P(\mathbf{x}) \ge \mathrm{I}_Q(\mathbf{x}), \mathrm{F}_P(\mathbf{x}) \ge \mathrm{F}_Q(\mathbf{x})$.

Definition 2.3. *[5, 42] Let there be two neutrosophic sets (NSs),*

$$P_{NS} = \{\langle \mathbf{x}, \mathrm{T}_P(\mathbf{x}), \mathrm{I}_P(\mathbf{x}), \mathrm{F}_P(\mathbf{x})\rangle : \mathbf{x} \in \mathbb{X}\}$$

and

$$Q_{NS} = \{\langle \mathbf{x}, \mathrm{T}_Q(\mathbf{x}), \mathrm{I}_Q(\mathbf{x}), \mathrm{F}_Q(\mathbf{x})\rangle : \mathbf{x} \in \mathbb{X}\}$$

then $P_{NS} = Q_{NS}$ *iff* $\mathrm{T}_P(\mathbf{x}) = \mathrm{T}_Q(\mathbf{x}), \mathrm{I}_P(\mathbf{x}) = \mathrm{I}_Q(\mathbf{x}), \mathrm{F}_P(\mathbf{x}) = \mathrm{F}_Q(\mathbf{x})$.

Definition 2.4. *[69] Let $\mathbb{X}$ be a space of objects with generic elements in $\mathbb{X}$ denoted by $\mathbf{x}$. A Single-Valued Neutrosophic set (SVNS) $\mathcal{A}$ in $\mathbb{X}$ is characterized by truth membership function* $\mathrm{T}_{\mathcal{A}}\mathbf{x}$, *indeterminacy membership function* $\mathrm{I}_{\mathcal{A}}\mathbf{x}$, *and falsity membership function* $\mathrm{F}_{\mathcal{A}}\mathbf{x}$. *For each point $\mathbf{x} \in \mathbb{X}$, there are* $\mathrm{T}_{\mathcal{A}}\mathbf{x}, \mathrm{I}_{\mathcal{A}}\mathbf{x}, \mathrm{F}_{\mathcal{A}}\mathbf{x} \in [0,1]$ *and* $0 \le \mathrm{T}_{\mathcal{A}}\mathbf{x} + \mathrm{I}_{\mathcal{A}}\mathbf{x} + \mathrm{F}_{\mathcal{A}}\mathbf{x} \le 3$. *Therefore, an SVNS $\mathcal{A}$ can be represented by*

$$\mathcal{A} = \{\langle \mathbf{x}, \mathrm{T}_{\mathcal{A}}\mathbf{x}, \mathrm{I}_{\mathcal{A}}\mathbf{x}, \mathrm{F}_{\mathcal{A}}\mathbf{x}\rangle | \mathbf{x} \in \mathbb{X}\}.$$

Definition 2.5. *[69] Let $\mathcal{A}$ be an SVNS over $\mathbb{X}$. Then complement of $\mathcal{A}$ is denoted by $\mathcal{A}^c$ and is defined as;*

$$\mathcal{A}^c = \{\langle \mathbf{x}, \mathrm{F}_{\mathcal{A}}\mathbf{x}, 1 - \mathrm{I}_{\mathcal{A}}\mathbf{x}, \mathrm{T}_{\mathcal{A}}\mathbf{x}\rangle | \mathbf{x} \in \mathbb{X}\}$$

3. Complex single-valued neutrosophic sets

Definition 3.1. *[70] A complex neutrosophic set S defined on a universe of discourse $\mathbb{X}$ is characterized by a truth membership function* $\mathrm{T}_S(\mathbf{x})$, *an indeterminacy membership function* $\mathrm{I}_S(\mathbf{x})$, *and a falsity membership function* $\mathrm{F}_S(\mathbf{x})$, *assigning complex-valued grades to each $\mathbf{x} \in \mathbb{X}$. The values* $\mathrm{T}_S(\mathbf{x})$, $\mathrm{I}_S(\mathbf{x})$, $\mathrm{F}_S(\mathbf{x})$ *and their sum lie within the unit circle in the complex plane and are given by*

$$\mathrm{T}_S(\mathbf{x}) = p_S(\mathbf{x})e^{j\mu_S(\mathbf{x})},$$
$$\mathrm{I}_S(\mathbf{x}) = q_S(\mathbf{x})e^{j\nu_S(\mathbf{x})},$$
$$\mathrm{F}_S(\mathbf{x}) = r_S(\mathbf{x})e^{j\omega_S(\mathbf{x})}.$$

where $p_S(\mathbf{x}), q_S(\mathbf{x}), r_S(\mathbf{x}) \in [0,1]$ *and* $\mu_S(\mathbf{x}), \nu_S(\mathbf{x}), \omega_S(\mathbf{x})$ *are real-valued functions such that*

$$0 \le p_S(\mathbf{x}) + q_S(\mathbf{x}) + r_S(\mathbf{x}) \le 3.$$

The complex neutrosophic set S can be represented as

$$S = \{\langle \mathbf{x}, \mathrm{T}_S(\mathbf{x}), \mathrm{I}_S(\mathbf{x}), \mathrm{F}_S(\mathbf{x})\rangle : \mathbf{x} \in \mathbb{X}\},$$

where

$$\mathrm{T}_S : \mathbb{X} \to \{a_\mathrm{T} \in \mathbb{C} : |a_\mathrm{T}| \le 1\}, \quad \mathrm{I}_S : \mathbb{X} \to \{a_\mathrm{I} \in \mathbb{C} : |a_\mathrm{I}| \le 1\},$$

$$\mathrm{F}_S : \mathbb{X} \to \{a_\mathrm{F} \in \mathbb{C} : |a_\mathrm{F}| \le 1\},$$

and

$$|\mathrm{T}_S(\mathbf{x})| + |\mathrm{I}_S(\mathbf{x})| + |\mathrm{F}_S(\mathbf{x})| \le 3.$$

The interval $(0, 2\pi]$ is chosen for the phase term to be in line with the original definition of a complex fuzzy set in which the amplitude terms lie in an interval of $(0, 1)$, and the phase terms lie in an interval of $(0, 2\pi]$.
Throughout the paper, a complex neutrosophic set refers to a neutrosophic set with complex-valued truth, indeterminacy, and falsity membership functions, while the classical neutrosophic set refers to the case where these membership functions are real-valued.

Remark 3.1. *In the definition above, ι denotes the imaginary number $\iota = \sqrt{-1}$ and it is this imaginary number ι that makes the CNS have complex-valued membership grades. The term $e^{\iota\theta}$ denotes the exponential form of a complex number and represents $e^{\iota\theta} = \cos\theta + \iota\sin\theta$.*

Definition 3.2. *Let there be two complex single-valued neutrosophic sets (CSVNSs),*

$$\mathcal{A}_{CSVNS} = \{\langle \mathbf{x}, \mathrm{T}_\mathcal{A}(\mathbf{x}), \mathrm{I}_\mathcal{A}(\mathbf{x}), \mathrm{F}_\mathcal{A}(\mathbf{x})\rangle : \mathbf{x} \in \mathbb{X}\}$$

and

$$\mathcal{B}_{CSVNS} = \{\langle \mathbf{x}, \mathrm{T}_\mathcal{B}(\mathbf{x}), \mathrm{I}_\mathcal{B}(\mathbf{x}), \mathrm{F}_\mathcal{B}(\mathbf{x})\rangle : \mathbf{x} \in \mathbb{X}\}$$

then $\mathcal{A}_{CSVNS} \subseteq \mathcal{B}_{CSVNS}$ iff $\mathrm{T}_\mathcal{A}(\mathbf{x}) \le \mathrm{T}_\mathcal{B}(\mathbf{x}), \mathrm{I}_\mathcal{A}(\mathbf{x}) \ge \mathrm{I}_\mathcal{B}(\mathbf{x}), \mathrm{F}_\mathcal{A}(\mathbf{x}) \ge \mathrm{F}_\mathcal{B}(\mathbf{x})$.

Definition 3.3. *Let there be complex single-valued neutrosophic sets (CSVNSs),*

$$\mathcal{A}_{CSVNS} = \{\langle \mathbf{x}, \mathrm{T}_\mathcal{A}(\mathbf{x}), \mathrm{I}_\mathcal{A}(\mathbf{x}), \mathrm{F}_\mathcal{A}(\mathbf{x})\rangle : \mathbf{x} \in \mathbb{X}\}$$

and

$$\mathcal{B}_{CSVNS} = \{\langle \mathbf{x}, \mathrm{T}_\mathcal{B}(\mathbf{x}), \mathrm{I}_\mathcal{B}(\mathbf{x}), \mathrm{F}_\mathcal{B}(\mathbf{x})\rangle : \mathbf{x} \in \mathbb{X}\}$$

then $\mathcal{A}_{CSVNS} = \mathcal{B}_{CSVNS}$ iff $\mathrm{T}_\mathcal{A}(\mathbf{x}) = \mathrm{T}_\mathcal{B}(\mathbf{x}), \mathrm{I}_\mathcal{A}(\mathbf{x}) = \mathrm{I}_\mathcal{B}(\mathbf{x}), \mathrm{F}_\mathcal{A}(\mathbf{x}) = \mathrm{F}_\mathcal{B}(\mathbf{x})$.

Definition 3.4. *Let $\mathcal{A}$ and $\mathcal{B}$ be two complex single-valued neutrosophic sets over the universe set $\mathbb{X}$. Then their union is represented by $A \cup \mathcal{B} = C$ is defined by:*

$$C = \{\langle \mathbf{x}, \mathrm{T}_C\mathbf{x}, \mathrm{I}_C\mathbf{x}, \mathrm{F}_C\mathbf{x}\rangle : \mathbf{x} \in \mathbb{X}\},$$

Where

$$\mathrm{T}_C\mathbf{x} = \max\{\mathrm{T}_\mathcal{A}\mathbf{x}, \mathrm{T}_\mathcal{B}\mathbf{x}\}$$

$$\mathrm{I}_C\mathbf{x} = \max\{\mathrm{I}_\mathcal{A}\mathbf{x}, \mathrm{I}_\mathcal{B}\mathbf{x}\}$$

$$\mathrm{F}_C\mathbf{x} = \min\{\mathrm{F}_\mathcal{A}\mathbf{x}, \mathrm{F}_\mathcal{B}\mathbf{x}\}$$

Definition 3.5. *Let $\mathcal{A}$ and $\mathcal{B}$ be two complex single-valued neutrosophic sets over the universe set $\mathbb{X}$. Then their intersection is represented by $A \cap \mathcal{B} = C$ is defined by:*

$$C = \{\langle \mathbf{x}, \mathrm{T}_C\mathbf{x}, \mathrm{I}_C\mathbf{x}, \mathrm{F}_C\mathbf{x}\rangle : \mathbf{x} \in \mathbb{X}\},$$

Where

$$\mathrm{T}_C\mathbf{x} = \min\{\mathrm{T}_\mathcal{A}\mathbf{x}, \mathrm{T}_\mathcal{B}\mathbf{x}\}$$

$$\mathrm{I}_C\mathbf{x} = \min\{\mathrm{I}_\mathcal{A}\mathbf{x}, \mathrm{I}_\mathcal{B}\mathbf{x}\}$$

$$\mathrm{F}_C\mathbf{x} = \max\{\mathrm{F}_\mathcal{A}\mathbf{x}, \mathrm{F}_\mathcal{B}\mathbf{x}\}$$

Definition 3.6. *Let $\{\mathcal{A}_i : i \in I\}$ be a family of complex single-valued neutrosophic sets over the universe set $\mathbb{X}$. Then,*

$$\bigcup_{i\in I} \mathcal{A}_i = \left\{\langle \mathbf{x}, \sup_{i\in I} \mathrm{T}_{\mathcal{A}_i}\mathbf{x}, \sup_{i\in I} \mathrm{I}_{\mathcal{A}_i}\mathbf{x}, \inf_{i\in I} \mathrm{F}_{\mathcal{A}_i}\mathbf{x}\rangle : \mathbf{x} \in \mathbb{X}\right\}.$$

$$\bigcap_{i\in I} \mathcal{A}_i = \left\{\langle \mathbf{x}, \inf_{i\in I} \mathrm{T}_{\mathcal{A}_i}\mathbf{x}, \inf_{i\in I} \mathrm{I}_{\mathcal{A}_i}\mathbf{x}, \sup_{i\in I} \mathrm{F}_{\mathcal{A}_i}()\rangle : \mathbf{x} \in \mathbb{X}\right\}.$$

Definition 3.7. *A complex single-valued neutrosophic set $\mathcal{A}$ over the universe set $\mathbb{X}$ is said to be a null complex single-valued neutrosophic set if*

$$\mathrm{T}_\mathcal{A}\mathbf{x} = 0, \quad \mathrm{I}_\mathcal{A}\mathbf{x} = 0, \quad \mathrm{F}_\mathcal{A}\mathbf{x} = 1, \quad \forall\, \mathbf{x} \in \mathbb{X}.$$

It is denoted by $0_\mathcal{A}$.

Definition 3.8. *A complex single-valued neutrosophic set $\mathcal{A}$ over the universe set $\mathbb{X}$ is said to be a absolute complex single-valued neutrosophic set if*

$$\mathrm{T}_\mathcal{A}\mathbf{x} = 1, \quad \mathrm{I}_\mathcal{A}\mathbf{x} = 1, \quad \mathrm{F}_\mathcal{A}\mathbf{x} = 0, \quad \forall\, \mathbf{x} \in \mathbb{X},$$

Clearly,

$$0^c_\mathcal{A} = 1_\mathcal{A}, \quad 1^c_\mathcal{A} = 0_\mathcal{A}.$$

Proposition 1. *Let $\mathcal{A}$, $\mathcal{B}$ and C be three complex single-valued neutrosophic sets over the universe set $\mathbb{X}$. Then,*

1. $\mathcal{A} \cup [\mathcal{B} \cup C] = [\mathcal{A} \cup \mathcal{B}] \cup C$ *and* $\mathcal{A} \cap [\mathcal{B} \cap C] = [\mathcal{A} \cap \mathcal{B}] \cap C$;
2. $\mathcal{A} \cup [\mathcal{B} \cap C] = [\mathcal{A} \cup \mathcal{B}] \cap [\mathcal{A} \cup C]$ *and* $\mathcal{A} \cap [\mathcal{B} \cup C] = [\mathcal{A} \cap \mathcal{B}] \cup [\mathcal{A} \cap C]$;
3. $\mathcal{A} \cup 0_\mathcal{A} = \mathcal{A}$ *and* $\mathcal{A} \cap 0_\mathcal{A} = 0_\mathcal{A}$;
4. $\mathcal{A} \cup 1_\mathcal{A} = 1_\mathcal{A}$ *and* $\mathcal{A} \cap 1_\mathcal{A} = \mathcal{A}$;

Proof. Let

$$\mathcal{A} = \{\langle \mathbf{x}, \mathrm{T}_\mathcal{A}(\mathbf{x}), \mathrm{I}_\mathcal{A}(\mathbf{x}), \mathrm{F}_\mathcal{A}(\mathbf{x})\rangle : \mathbf{x} \in \mathbb{X}\},$$

$$\mathcal{B} = \{\langle \mathbf{x}, \mathrm{T}_\mathcal{B}(\mathbf{x}), \mathrm{I}_\mathcal{B}(\mathbf{x}), \mathrm{F}_\mathcal{B}(\mathbf{x})\rangle : \mathbf{x} \in \mathbb{X}\},$$

$$C = \{\langle \mathbf{x}, \mathrm{T}_C(\mathbf{x}), \mathrm{I}_C(\mathbf{x}), \mathrm{F}_C(\mathbf{x})\rangle : \mathbf{x} \in \mathbb{X}\}.$$

1. For any $\mathbf{x} \in \mathbb{X}$,

$$\begin{aligned}\mathcal{A} \cup (\mathcal{B} \cup C) = \{\langle \mathbf{x}, &\max(\mathrm{T}_{\mathcal{A}}, \max(\mathrm{T}_{\mathcal{B}}, \mathrm{T}_{C})),\\ &\min(\mathrm{I}_{\mathcal{A}}, \min(\mathrm{I}_{\mathcal{B}}, \mathrm{I}_{C})),\\ &\min(\mathrm{F}_{\mathcal{A}}, \min(\mathrm{F}_{\mathcal{B}}, \mathrm{F}_{C}))\rangle\}\end{aligned}$$

$$\begin{aligned}= \{\langle \mathbf{x}, &\max(\max(\mathrm{T}_{\mathcal{A}}, \mathrm{T}_{\mathcal{B}}), \mathrm{T}_{C}),\\ &\min(\min(\mathrm{I}_{\mathcal{A}}, \mathrm{I}_{\mathcal{B}}), \mathrm{I}_{C}),\\ &\min(\min(\mathrm{F}_{\mathcal{A}}, \mathrm{F}_{\mathcal{B}}), \mathrm{F}_{C})\rangle\}\\ = (\mathcal{A} &\cup \mathcal{B}) \cup C.\end{aligned}$$

Similarly,
$$\mathcal{A} \cap (\mathcal{B} \cap C) = (\mathcal{A} \cap \mathcal{B}) \cap C.$$

2. For any $\mathbf{x} \in \mathbb{X}$,

$$\begin{aligned}\mathcal{A} \cup (\mathcal{B} \cap C) = \{\langle \mathbf{x}, &\max(\mathrm{T}_{\mathcal{A}}, \min(\mathrm{T}_{\mathcal{B}}, \mathrm{T}_{C})),\\ &\min(\mathrm{I}_{\mathcal{A}}, \max(\mathrm{I}_{\mathcal{B}}, \mathrm{I}_{C})),\\ &\min(\mathrm{F}_{\mathcal{A}}, \max(\mathrm{F}_{\mathcal{B}}, \mathrm{F}_{C}))\rangle\}\end{aligned}$$

$$\begin{aligned}= \{\langle \mathbf{x}, &\min(\max(\mathrm{T}_{\mathcal{A}}, \mathrm{T}_{\mathcal{B}}), \max(\mathrm{T}_{\mathcal{A}}, \mathrm{T}_{C})),\\ &\max(\min(\mathrm{I}_{\mathcal{A}}, \mathrm{I}_{\mathcal{B}}), \min(\mathrm{I}_{\mathcal{A}}, \mathrm{I}_{C})),\\ &\max(\min(\mathrm{F}_{\mathcal{A}}, \mathrm{F}_{\mathcal{B}}), \min(\mathrm{F}_{\mathcal{A}}, \mathrm{F}_{C}))\rangle\}\\ = (\mathcal{A} &\cup \mathcal{B}) \cap (\mathcal{A} \cup C).\end{aligned}$$

Similarly,

$$\mathcal{A} \cap (\mathcal{B} \cup C) = (\mathcal{A} \cap \mathcal{B}) \cup (\mathcal{A} \cap C).$$

3. Let $0_{\mathcal{A}} = \{\langle \mathbf{x}, 0, 1, 1\rangle : \mathbf{x} \in \mathbb{X}\}$. Then

$$\begin{aligned}\mathcal{A} \cup 0_{\mathcal{A}} &= \{\langle \mathbf{x}, \max(\mathrm{T}_{\mathcal{A}}, 0), \min(\mathrm{I}_{\mathcal{A}}, 1), \min(\mathrm{F}_{\mathcal{A}}, 1)\rangle\}\\ &= \mathcal{A},\end{aligned}$$

$$\begin{aligned}\mathcal{A} \cap 0_{\mathcal{A}} &= \{\langle \mathbf{x}, \min(\mathrm{T}_{\mathcal{A}}, 0), \max(\mathrm{I}_{\mathcal{A}}, 1), \max(\mathrm{F}_{\mathcal{A}}, 1)\rangle\}\\ &= 0_{\mathcal{A}}.\end{aligned}$$

4. Let $1_{\mathcal{A}} = \{\langle \mathbf{x}, 1, 0, 0\rangle : \mathbf{x} \in \mathbb{X}\}$. Then

$$\begin{aligned}\mathcal{A} \cup 1_{\mathcal{A}} &= \{\langle \mathbf{x}, \max(\mathrm{T}_{\mathcal{A}}, 1), \min(\mathrm{I}_{\mathcal{A}}, 0), \min(\mathrm{F}_{\mathcal{A}}, 0)\rangle\}\\ &= 1_{\mathcal{A}},\end{aligned}$$

$$\begin{aligned}\mathcal{A} \cap 1_{\mathcal{A}} &= \{\langle \mathbf{x}, \min(\mathrm{T}_{\mathcal{A}}, 1), \max(\mathrm{I}_{\mathcal{A}}, 0), \max(\mathrm{F}_{\mathcal{A}}, 0)\rangle\}\\ &= \mathcal{A}.\end{aligned}$$

□

Proposition 2. *Let $\mathcal{A}$ and $\mathcal{B}$ be two complex single-valued neutrosophic sets over the universe set $\mathbb{X}$. Then,*

1. $[\mathcal{A} \cup \mathcal{B}]^c = A^c \cap \mathcal{B}^c$
2. $[\mathcal{A} \cap \mathcal{B}]^c = A^c \cup \mathcal{B}^c$

Proof. (i). For all $\mathbf{x} \in \mathbb{X}$,

$$\begin{aligned}\mathcal{A} \cup \mathcal{B} &= \{\langle \mathbf{x}, \max\{\mathrm{T}_{\mathcal{A}}\mathbf{x}, \mathrm{T}_{\mathcal{B}}\mathbf{x}\}, \max\{\mathrm{I}_{\mathcal{A}}\mathbf{x}, \mathrm{I}_{\mathcal{B}}\mathbf{x}\},\\ &\quad \min\{\mathrm{F}_{\mathcal{A}}\mathbf{x}, \mathrm{F}_{\mathcal{B}}\mathbf{x}\}\rangle\}\\ [\mathcal{A} \cup \mathcal{B}]^c &= \{\langle \mathbf{x}, \min\{\mathrm{F}_{\mathcal{A}}\mathbf{x}, \mathrm{F}_{\mathcal{B}}\mathbf{x}\}, 1 - \max\{\mathrm{I}_{\mathcal{A}}\mathbf{x}, \mathrm{I}_{\mathcal{B}}\mathbf{x}\},\\ &\quad \max\{\mathrm{T}_{\mathcal{A}}\mathbf{x}, \mathrm{T}_{\mathcal{B}}\mathbf{x}\}\rangle\}\end{aligned}$$

Now,

$$\begin{aligned}\mathcal{A}^c &= \{\langle \mathbf{x}, \mathrm{F}_{\mathcal{A}}\mathbf{x}, 1 - \mathrm{I}_{\mathcal{A}}\mathbf{x}, \mathrm{T}_{\mathcal{A}}\mathbf{x}\rangle\}\\ \mathcal{B}^c &= \{\langle \mathbf{x}, \mathrm{F}_{\mathcal{B}}\mathbf{x}, 1 - \mathrm{I}_{\mathcal{B}}\mathbf{x}, \mathrm{T}_{\mathcal{B}}\mathbf{x}\rangle\}\end{aligned}$$

Then,

$$\begin{aligned}\mathcal{A}^c \cap \mathcal{B}^c &= \{\langle \mathbf{x}, \min\{\mathrm{F}_{\mathcal{A}}\mathbf{x}, \mathrm{F}_{\mathcal{B}}\mathbf{x}\}, \min\{1 - \mathrm{I}_{\mathcal{A}}\mathbf{x}, 1 - \mathrm{I}_{\mathcal{B}}\mathbf{x}\},\\ &\quad \max\{\mathrm{T}_{\mathcal{A}}\mathbf{x}, \mathrm{T}_{\mathcal{B}}\mathbf{x}\}\rangle\}\\ &= \{\langle \mathbf{x}, \min\{\mathrm{F}_{\mathcal{A}}\mathbf{x}, \mathrm{F}_{\mathcal{B}}\mathbf{x}\}, 1 - \max\{\mathrm{I}_{\mathcal{A}}\mathbf{x}, \mathrm{I}_{\mathcal{B}}\mathbf{x}\},\\ &\quad \max\{\mathrm{T}_{\mathcal{A}}\mathbf{x}, \mathrm{T}_{\mathcal{B}}\mathbf{x}\}\rangle\}\end{aligned}$$

Therefore, $[\mathcal{A} \cup \mathcal{B}]^c = \mathcal{A}^c \cap \mathcal{B}^c$.
(ii). It is obtained in a similar way. □

Example 3.1. *Suppose that, the universe set $\mathbb{X}$ given by $\mathbb{X} = \{\mathbf{x}_1, \mathbf{x}_2, \mathbf{x}_3, \mathbf{x}_4\}$. Let us consider complex single-valued neutrosophic sets $\mathcal{A}$ and $\mathcal{B}$ over the universe set $\mathbb{X}$ as follows*

$$\mathcal{A} = \begin{bmatrix} (\langle x_1, 0.3e^{\iota\pi(0.2)}, 0.4e^{\iota\pi(0.3)}, 0.6e^{\iota\pi(0.5)}\rangle, \\ \langle x_2, 0.4e^{\iota\pi(0.3)}, 0.2e^{\iota\pi(0.1)}, 0.8e^{\iota\pi(0.7)}\rangle, \\ \langle x_3, 0.6e^{\iota\pi(0.5)}, 0.2e^{\iota\pi(0.1)}, 0.5e^{\iota\pi(0.4)}\rangle, \\ \langle x_4, 0.2e^{\iota\pi(0.1)}, 0.3e^{\iota\pi(0.2)}, 0.4e^{\iota\pi(0.3)}\rangle) \\ (\langle x_1, 0.4e^{\iota\pi(0.3)}, 0.3e^{\iota\pi(0.2)}, 0.8e^{\iota\pi(0.7)}\rangle, \\ \langle x_2, 0.3e^{\iota\pi(0.2)}, 0.4e^{\iota\pi(0.3)}, 0.2e^{\iota\pi(0.1)}\rangle, \\ \langle x_3, 0.3e^{\iota\pi(0.2)}, 0.2e^{\iota\pi(0.1)}, 0.7e^{\iota\pi(0.6)}\rangle, \\ \langle x_4, 0.1e^{\iota\pi(0.1)}, 0.2e^{\iota\pi(0.1)}, 0.9e^{\iota\pi(0.8)}\rangle) \end{bmatrix}$$

$$\mathcal{B} = \begin{bmatrix} (\langle x_1, 0.6e^{\iota\pi(0.5)}, 0.3e^{\iota\pi(0.2)}, 0.8e^{\iota\pi(0.7)}\rangle, \\ \langle x_2, 0.2e^{\iota\pi(0.1)}, 0.5e^{\iota\pi(0.4)}, 0.8e^{\iota\pi(0.7)}\rangle, \\ \langle x_3, 0.1e^{\iota\pi(0.1)}, 0.1e^{\iota\pi(0.1)}, 0.4e^{\iota\pi(0.3)}\rangle, \\ \langle x_4, 0.5e^{\iota\pi(0.4)}, 0.2e^{\iota\pi(0.1)}, 0.3e^{\iota\pi(0.2)}\rangle) \\ (\langle x_1, 0.7e^{\iota\pi(0.6)}, 0.5e^{\iota\pi(0.4)}, 0.6e^{\iota\pi(0.5)}\rangle, \\ \langle x_2, 0.4e^{\iota\pi(0.3)}, 0.2e^{\iota\pi(0.1)}, 0.3e^{\iota\pi(0.2)}\rangle, \\ \langle x_3, 0.5e^{\iota\pi(0.4)}, 0.3e^{\iota\pi(0.2)}, 0.4e^{\iota\pi(0.3)}\rangle, \\ \langle x_4, 0.4e^{\iota\pi(0.3)}, 0.2e^{\iota\pi(0.1)}, 0.6e^{\iota\pi(0.5)}\rangle) \end{bmatrix}$$

Then, their union and intersection operations are given as follows:

$$\mathcal{A} \cup \mathcal{B} = \begin{bmatrix} (\langle x_1, 0.6e^{\iota\pi(0.5)}, 0.4e^{\iota\pi(0.3)}, 0.6e^{\iota\pi(0.5)}\rangle, \\ \langle x_2, 0.4e^{\iota\pi(0.3)}, 0.5e^{\iota\pi(0.4)}, 0.8e^{\iota\pi(0.7)}\rangle, \\ \langle x_3, 0.6e^{\iota\pi(0.5)}, 0.2e^{\iota\pi(0.1)}, 0.4e^{\iota\pi(0.3)}\rangle, \\ \langle x_4, 0.5e^{\iota\pi(0.4)}, 0.3e^{\iota\pi(0.2)}, 0.3e^{\iota\pi(0.2)}\rangle) \\ (\langle x_1, 0.7e^{\iota\pi(0.6)}, 0.5e^{\iota\pi(0.4)}, 0.6e^{\iota\pi(0.5)}\rangle, \\ \langle x_2, 0.4e^{\iota\pi(0.3)}, 0.4e^{\iota\pi(0.3)}, 0.2e^{\iota\pi(0.1)}\rangle, \\ \langle x_3, 0.5e^{\iota\pi(0.4)}, 0.3e^{\iota\pi(0.2)}, 0.4e^{\iota\pi(0.3)}\rangle, \\ \langle x_4, 0.4e^{\iota\pi(0.3)}, 0.2e^{\iota\pi(0.1)}, 0.6e^{\iota\pi(0.5)}\rangle) \end{bmatrix}$$

$$\mathcal{A} \cap \mathcal{B} = \begin{bmatrix} (\langle x_1, 0.3e^{\iota\pi(0.2)}, 0.3e^{\iota\pi(0.3)}, 0.8e^{\iota\pi(0.7)}\rangle, \\ \langle x_2, 0.2e^{\iota\pi(0.1)}, 0.2e^{\iota\pi(0.1)}, 0.8e^{\iota\pi(0.7)}\rangle, \\ \langle x_3, 0.1e^{\iota\pi(0.1)}, 0.1e^{\iota\pi(0.1)}, 0.5e^{\iota\pi(0.4)}\rangle, \\ \langle x_4, 0.2e^{\iota\pi(0.1)}, 0.2e^{\iota\pi(0.2)}, 0.4e^{\iota\pi(0.4)}\rangle) \\ (\langle x_1, 0.3e^{\iota\pi(0.2)}, 0.3e^{\iota\pi(0.3)}, 0.8e^{\iota\pi(0.7)}\rangle, \\ \langle x_2, 0.2e^{\iota\pi(0.1)}, 0.2e^{\iota\pi(0.1)}, 0.8e^{\iota\pi(0.7)}\rangle, \\ \langle x_3, 0.1e^{\iota\pi(0.1)}, 0.1e^{\iota\pi(0.1)}, 0.5e^{\iota\pi(0.4)}\rangle, \\ \langle x_4, 0.2e^{\iota\pi(0.1)}, 0.2e^{\iota\pi(0.2)}, 0.4e^{\iota\pi(0.3)}\rangle) \end{bmatrix}$$

4. Cotangent similarity measures for complex single-valued neutrosophic sets

Let $\mathcal{A} = \langle \mathbf{x}, \mathrm{T}_{\mathcal{A}}\mathbf{x}, \mathrm{I}_{\mathcal{A}}\mathbf{x}, \mathrm{F}_{\mathcal{A}}\mathbf{x}\rangle$ and $\mathcal{B} = \langle \mathbf{x}, \mathrm{T}_{\mathcal{B}}\mathbf{x}, \mathrm{I}_{\mathcal{B}}\mathbf{x}, \mathrm{F}_{\mathcal{B}}\mathbf{x}\rangle$ be two Complex single-valued neutrosophic numbers. Now cotangent similarity function which measures the similarity between two vectors based only on the direction, ignoring the impact of the distance between them can be presented as follows:

$$Cotangent_{CSVNS}(\mathcal{A}, \mathcal{B}) = \frac{1}{n}\sum_{k=1}^{n}\{\cot[\frac{\pi}{4} + \frac{\pi}{12}(|\mathrm{T}_{ik} - \mathrm{T}_{jk}| + |\mathrm{I}_{ik} - \mathrm{I}_{jk}| + |\mathrm{F}_{ik} - \mathrm{F}_{jk}|)]\}$$

Proposition 3. *Cotangent similarity measure $Cot_{CSVNS}(\mathcal{A}, \mathcal{B})$ between $\mathcal{A}$ and $\mathcal{B}$ satisfies the following properties:*

1. $0 \le Cot_{CSVNS}(\mathcal{A}, \mathcal{B}) \le 1$.
2. $Cot_{CSVNS}(\mathcal{A}, \mathcal{B}) = 1$ *iff* $A = \mathcal{B}$.
3. $Cot_{CSVNS}(\mathcal{A}, \mathcal{B}) = Cot_{CNRS}(\mathcal{B}, \mathcal{A})$.
4. *If R is a CSVNS in $\mathbb{X}$ and $\mathcal{A} \subset \mathcal{B} \subset C$ then $Cot_{CSVNS}(\mathcal{A}, C) \le Cot_{CSVNS}(\mathcal{A}, \mathcal{B})$ and $Cot_{CSVNS}(\mathcal{A}, C) \le Cot_{CSVNS}(\mathcal{B}, C)$.*

Proof.

1. As the truth-membership, indeterminacy membership and False-membership functions of the CSVNSs and the value of the cotangent function are within $[0, 1]$, the similarity measure based on cotangent function also within $[0, 1]$. Hence $0 \le Cot_{CSVNS}(\mathcal{A}, \mathcal{B}) \le 1$.
2. For any two CSVNS $\mathcal{A}$ and $\mathcal{B}$ if $\mathcal{A} = \mathcal{B}$, this implies $\mathrm{T}_{\mathcal{A}}\mathbf{x} = \mathrm{T}_{\mathcal{B}}\mathbf{x}, \mathrm{I}_{\mathcal{A}}\mathbf{x} = \mathrm{I}_{\mathcal{B}}\mathbf{x}, \mathrm{F}_{\mathcal{A}}\mathbf{x} = \mathrm{F}_{\mathcal{B}}\mathbf{x}$. Hence $|\mathrm{T}_{\mathcal{A}}\mathbf{x} - \mathrm{T}_{\mathcal{B}}\mathbf{x}| = 0, |\mathrm{I}_{\mathcal{A}}\mathbf{x} - \mathrm{I}_{\mathcal{B}}\mathbf{x}| = 0, |\mathrm{F}_{\mathcal{A}}\mathbf{x} - \mathrm{F}_{\mathcal{B}}\mathbf{x}| = 0$. Thus $Cot_{CSVNS}(\mathcal{A}, \mathcal{B}) = 1$.
   Conversely, If $Cot_{CSVNS}(\mathcal{A}, \mathcal{B}) = 1$ then $|\mathrm{T}_{\mathcal{A}}\mathbf{x} - \mathrm{T}_{\mathcal{B}}\mathbf{x}| = 0, |\mathrm{I}_{\mathcal{A}}\mathbf{x} - \mathrm{I}_{\mathcal{B}}\mathbf{x}| = 0, |\mathrm{F}_{\mathcal{A}}\mathbf{x} - \mathrm{F}_{\mathcal{B}}\mathbf{x}| = 0$ since $\tan(0) = 0$.
   So we can we can write, $\mathrm{T}_{\mathcal{A}}\mathbf{x} = \mathrm{T}_{\mathcal{B}}\mathbf{x}, \mathrm{I}_{\mathcal{A}}\mathbf{x} = \mathrm{I}_{\mathcal{B}}\mathbf{x}, \mathrm{F}_{\mathcal{A}}\mathbf{x} = \mathrm{F}_{\mathcal{B}}\mathbf{x}$. Hence $\mathcal{A} = \mathcal{B}$.
3. For each $\mathbf{x} \in \mathbb{X}$, using the property of absolute value, we have
   $$|\mathrm{T}_{\mathcal{A}}(\mathbf{x}) - \mathrm{T}_{\mathcal{B}}(\mathbf{x})| = |\mathrm{T}_{\mathcal{B}}(\mathbf{x}) - \mathrm{T}_{\mathcal{A}}(\mathbf{x})|,$$
   $$|\mathrm{I}_{\mathcal{A}}(\mathbf{x}) - \mathrm{I}_{\mathcal{B}}(\mathbf{x})| = |\mathrm{I}_{\mathcal{B}}(\mathbf{x}) - \mathrm{I}_{\mathcal{A}}(\mathbf{x})|,$$
   $$|\mathrm{F}_{\mathcal{A}}(\mathbf{x}) - \mathrm{F}_{\mathcal{B}}(\mathbf{x})| = |\mathrm{F}_{\mathcal{B}}(\mathbf{x}) - \mathrm{F}_{\mathcal{A}}(\mathbf{x})|.$$
   Adding these equalities yields
   $$|\mathrm{T}_{\mathcal{A}}(\mathbf{x}) - \mathrm{T}_{\mathcal{B}}(\mathbf{x})| + |\mathrm{I}_{\mathcal{A}}(\mathbf{x}) - \mathrm{I}_{\mathcal{B}}(\mathbf{x})| + |\mathrm{F}_{\mathcal{A}}(\mathbf{x}) - \mathrm{F}_{\mathcal{B}}(\mathbf{x})|$$
   $$=|\mathrm{T}_{\mathcal{B}}(\mathbf{x}) - \mathrm{T}_{\mathcal{A}}(\mathbf{x})| + |\mathrm{I}_{\mathcal{B}}(\mathbf{x}) - \mathrm{I}_{\mathcal{A}}(\mathbf{x})| + |\mathrm{F}_{\mathcal{B}}(\mathbf{x}) - \mathrm{F}_{\mathcal{A}}(\mathbf{x})|.$$
   Hence, the argument inside the cotangent function is identical in both definitions for every $\mathbf{x} \in \mathbb{X}$. Therefore,
   $$Cot_{CSVNS}(\mathcal{A}, \mathcal{B}) = Cot_{CNRS}(\mathcal{B}, \mathcal{A}).$$
4. If $\mathcal{A} \subset \mathcal{B} \subset C$ then $\mathrm{T}_{\mathcal{A}}\mathbf{x} \le \mathrm{T}_{\mathcal{B}}\mathbf{x} \le \mathrm{T}_{R}\mathbf{x}$, $\mathrm{I}_{\mathcal{A}}\mathbf{x} \ge \mathrm{I}_{\mathcal{B}}\mathbf{x} \ge \mathrm{I}_{R}\mathbf{x}$, and $\mathrm{F}_{\mathcal{A}}\mathbf{x} \ge \mathrm{F}_{\mathcal{B}}\mathbf{x} \ge \mathrm{F}_{R}\mathbf{x}$ for $\mathbf{x} \in \mathbb{X}$. Now we have the following inequalities:
   $|\mathrm{T}_{\mathcal{A}}\mathbf{x} - \mathrm{T}_{\mathcal{B}}\mathbf{x}| \le |\mathrm{T}_{\mathcal{A}}\mathbf{x} - \mathrm{T}_{R}\mathbf{x}|, |\mathrm{T}_{\mathcal{B}}\mathbf{x} - \mathrm{T}_{R}\mathbf{x}| \le |\mathrm{T}_{\mathcal{A}}\mathbf{x} - \mathrm{T}_{R}\mathbf{x}|$;
   $|\mathrm{I}_{\mathcal{A}}\mathbf{x} - \mathrm{I}_{\mathcal{B}}\mathbf{x}| \le |\mathrm{I}_{\mathcal{A}}\mathbf{x} - \mathrm{T}_{R}\mathbf{x}|, |\mathrm{I}_{\mathcal{B}}\mathbf{x} - \mathrm{I}_{R}\mathbf{x}| \le |\mathrm{I}_{\mathcal{A}}\mathbf{x} - \mathrm{I}_{R}\mathbf{x}|$;
   $|\mathrm{F}_{\mathcal{A}}\mathbf{x} - \mathrm{F}_{\mathcal{B}}\mathbf{x}| \le |\mathrm{F}_{\mathcal{A}}\mathbf{x} - \mathrm{F}_{R}\mathbf{x}|, |\mathrm{F}_{\mathcal{B}}\mathbf{x} - \mathrm{F}_{R}\mathbf{x}| \le |\mathrm{F}_{\mathcal{A}}\mathbf{x} - \mathrm{F}_{R}\mathbf{x}|$;
   Thus $Cot_{CSVNS}(\mathcal{A}, C) \le Cot_{CSVNS}(\mathcal{A}, \mathcal{B})$ and $Cot_{CSVNS}(\mathcal{A}, C) \le Cot_{CSVNS}(\mathcal{B}, C)$. The cotangent function is decreasing function within the interval $[\frac{\pi}{4}, \frac{\pi}{2}]$.

□

5. Encrypted visual analytics for high-dimensional data exploration

Encryption is a key component of the proposed visual analytics system, as it guarantees privacy-preserving data analysis. In this research, the values of the numerical features are encrypted before dimensionality reduction, visualization and correlation analysis. This ensures that the underlying data is never revealed, even when exploring the data. The main benefit of using encryption is the ability to explore data in a secure and privacy-preserving manner. Existing methods for data visualization and machine learning typically assume access to the raw values, which is potentially problematic when dealing with sensitive data like medical data, surveillance data or confidential data. In contrast, the new method is completely based on encrypted feature spaces, maintaining privacy throughout the process. The encryption of data does not compromise the relational properties of the data. Methods like t-SNE retain the local neighborhood structure, enabling meaningful clustering and class separations to be detected, despite the hidden values. Likewise, encrypted Pearson correlation preserves the direction and magnitude of relationships between variables, allowing reliable inferences while preserving privacy.

Encryption is crucial in the context of:

- Data Privacy and Security: It ensures data security and protects against data breaches by hiding original feature values.
- Compliance: Many new data privacy laws require stringent measures to protect sensitive data; encryption helps satisfy these requirements.
- Collaborative Security: Encrypted analytics enables collaborative analysis of shared data without sharing sensitive data.
- Privacy-Enhanced AI: Incorporating privacy protection methods, the approach increases trust in the results and encourages ethical data practices. Moreover, encryption, coupled with normalization, allows for comparisons between dimensions while hiding their absolute values. This trade-off between privacy and interpretability is essential because it enables analysts to discover patterns, identify anomalies and comprehend class structures while preserving privacy.

In conclusion, encryption is not just a security measure but an integral part of the proposed approach. It facilitates a new era of privacy-preserving visual analytics, in which insightful information can be obtained from multidimensional data while ensuring privacy. It shows that effective analytics and unprecedented data privacy can be achieved in a single framework.

This section describes a visual analytics methodology for secure exploration of fully encrypted high-dimensional data that preserves privacy. The projected encrypted feature vectors are placed in a three-dimensional latent space using t-distributed Stochastic Neighbor Embedding (t-SNE) in order to conceal original values and maintain local structure. To make the scales comparable across the encrypted dimensions, minimum maximum normalization is applied. Analysis of defects The class structure, dispersion, and overlap are examined using a 3D scatter plot and parallel coordinates DSS. Since the support items do not disclose numerical magnitudes, encrypted Pearson correlation analysis is used to analyze the inter-variable correlations with the help of Heatmap representations. The results demonstrate that even in the case of encoding, important structural and connection patterns can still be understood. The proposed framework would enable effective exploratory analysis and visualization of sensitive data while maintaining data privacy.

The following techniques are employed by the suggested encrypted visual analytics framework.

t-Distributed stochastic neighbor embedding (t-SNE). t-SNE is used to project the high-dimensional encrypted feature data into a three-dimensional latent space without altering local neighborhood interactions in order to reduce the dimensionality of the data in a non-linear way [71].

3D t-SNE visualization. In order to properly interpret the embedded data into space and observe the structure and dispersion of classes in the encrypted embeddings, the t-SNE is expanded to three dimensions [71].

Data encryption for privacy preservation. To conceal the original numerical values and maintain the relative structural relationships required for the study, they are encrypted prior to analysis [72].

Privacy-preserving data analytics. The system complies with privacy-preserving data mining concepts, which enable exploratory analysis, clustering, and visualization of encrypted datasets without disclosing any private information [73].

Min–max normalization (0–1 scaling). Normalization of encrypted embeddings and correlation values improves their comparability in visualization and ensures consistency across-dimension scales [74].

Parallel coordinates visualization. The patterns of variance, dispersion, and inter-class overlap on the t-SNE dimensions of the multidimensional encrypted embeddings are examined using parallel coordinates plots [75].

Secure visualization techniques. To maintain interpretability without going against encryption policies, visualization technologies that support a security-sensitive data environment are employed [76].

Pearson correlation analysis. To quantify the line associations of encrypted targets and signals and preserve relational integrity, encrypted Pearson correlation coefficients are computed [77].

Correlation heatmap visualization. Heatmaps are a visual representation of encrypted correlation matrices that facilitate the rapid identification of dominating associations and the easy identification of comparison trends [78].

Normalized encrypted correlation analysis. This is due to the fact that normalization and encryption offer full numerical confidentiality and enable interpretable comparison of correlation strengths [79].

5.1. *Cotangent similarity measure [80]*

Let $\mathrm{T}_i = (\mathrm{T}_{ik}, \mathrm{I}_{ik}, \mathrm{F}_{ik})$ and $C_j = (\mathrm{T}_{jk}, \mathrm{I}_{jk}, \mathrm{F}_{jk})$ be two CSVNSs. Each set is represented by three components for each feature k:
T_{ik}: Truth-membership of feature k for T_i.
I_{ik}: Indeterminacy-membership of feature k for T_i.
F_{ik}: Falsity-membership degree of feature k for T_i.
The values typically satisfy: $\mathrm{T}_{ik}, \mathrm{I}_{ik}, \mathrm{F}_{ik} \in [0, 1]$
Similarly, for object C_j:
T_{jk}: Truth-membership of feature k for C_j.
I_{jk}: Indeterminacy-membership of feature k for C_j.
F_{jk}: Falsity-membership degree of feature k for C_j.
The values typically satisfy: $\mathrm{T}_{jk}, \mathrm{I}_{jk}, \mathrm{F}_{jk} \in [0, 1]$.
The cotangent similarity measure between T_i and C_j is defined as:

$$Cotangent_{CSVNS}(\mathrm{T}_i, C_j) =$$
$$\frac{1}{n}\sum_{k=1}^{n}\{\cot[\frac{\pi}{4} + \frac{\pi}{12}(|\mathrm{T}_{ik} - \mathrm{T}_{jk}| + |\mathrm{I}_{ik} - \mathrm{I}_{jk}| + |\mathrm{F}_{ik} - \mathrm{F}_{jk}|)]\}$$

5.2. *Complex neutrosophic set-driven cotangent similarity model for ambiguous signal interpretation [80]*

The task of target classification in today's surveillance and reconnaissance systems is complicated by the nature of multi-source signal data. Signals like thermal radiation, radar returns, and electronic measurements are frequently uncertain, fuzzy and partially overlapping, with different degrees of reliability and non-linear connections between features. These factors make it challenging to compare observed signals, operational targets, and classes.

This paper presents a cotangent similarity model designed in the Complex Single-Valued Neutrosophic Set (CSVNS) environment that adequately deals with these problems. The proposed method uses three components (truth-membership, indeterminacy-membership, and falsity-membership) to define each target-class pair, enabling it to model uncertainty more fully. The use of complex information allows the model to consider both the amplitude and phase of the information. The difference between targets and operational classes is assessed using a normalized measure and then converted using a cotangent function to obtain similarity measures in a fixed interval. The similarity measures are then used to rank and classify targets to the corresponding operational classes.

This approach improves the efficiency and reliability of decision-making in uncertain, ambiguous situations, and is a useful technique for advanced signal interpretation and target classification systems.

Numerical illustrative example. [80] Using the multi-source signal samples $S = \{S_1, S_2, S_3\}$ to accurately categorize the operational targets $T = \{\mathrm{T}_1, \mathrm{T}_2, \mathrm{T}_3\}$ and then applying them to the appropriate operational classes $C = \{C_1, C_2, C_3\}$ is the primary task in the current surveillance and reconnaissance systems. The available information on each target is inherently ambiguous, imprecise, and diverse; it includes heat emissions, radar signatures, electronic monitoring, and other signal measures. This uncertainty necessitates a mathematical procedure that can simultaneously handle truth, indeterminacy, and falsity. The relationship between targets, signals, and classes in a multi-faceted environment is related in terms of event-based measures (e) and their corresponding measures in the operational classification table (Table 2). However, overlapping values, inconsistent reliability, and nonlinear relationships between features make it impossible to directly compare a response of raw signals between targets and classes. This is resolved by proposing a Cotangent similarity measure based on the complex neutrosophic soft set (Cotangent CSVNS) framework, which enables the measurement of each

target-class pair's similarity. It considers the joint contribution of the truth-membership, indeterminacy-membership, and falsity-membership functions, normalized with respect to $n = 3$ attributes, in each pair (T_i, C_j). Cotangent similarity scores are generated as a result, and these can be used to rank candidate target profiles in relation to operational class templates.

All target-classification pairings are then averaged by adding the cotangent values that were determined for each pair of targets and categorized profiles.

The values of the resulting cotangent similarity:

$Cotangent_{CSVNS}(T_1, C_1) = 0.4913$
$Cotangent_{CSVNS}(T_1, C_2) = 0.6653$
$Cotangent_{CSVNS}(T_1, C_3) = 0.5785$
$Cotangent_{CSVNS}(T_1, C_1) = 0.5287$
$Cotangent_{CSVNS}(T_1, C_2) = 0.4937$
$Cotangent_{CSVNS}(T_1, C_3) = 0.3576$
$Cotangent_{CSVNS}(T_1, C_1) = 0.4110$
$Cotangent_{CSVNS}(T_1, C_2) = 0.4604$
$Cotangent_{CSVNS}(T_1, C_3) = 0.4221$

6. Results and discussion

The 3D Encrypted Parallel Coordinates Figure 1 plot shows that, the similarity values of the cotangents of $T_1 - T_3$ in the regions $S_1 - S_3$ are preserved after encryption but with a small amount of controlled perturbation. The solid lines are the original normalized similarities while the dashed lines are the encrypted values, indicating that the relative similarity patterns are preserved after the encryption process.

The graph also shows the best matching pairs, $T_1 \rightarrow S_2$ (0.6653), $T_2 \rightarrow S_1$ (0.5287), and $T_3 \rightarrow S_2$ (0.4604), which means that the encryption does not affect the underlying decision relationships. The noise in the encrypted region (±0.0309)

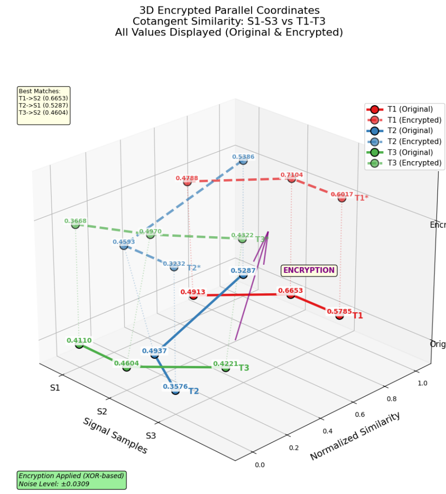

Figure 1. 3D Encrypted Parallel Coordinates

is displayed, which results in minor deviations in the encrypted coordinates, thus demonstrating that the proposed encryption scheme preserves the similarity data while maintaining its analytical value.

In conclusion, the visualization demonstrates that the encryption mechanism provides a good balance of data confidentiality and information preservation, which is suitable for privacy-preserving decision-making applications and secure similarity analysis.

The behavior of the Min-Max normalized cotangent similarity values before and after encryption is plotted in the 3D Encrypted Parallel Coordinates (Normalized Data) Figure 2 plot. All the similarity scores are scaled to the range [0,1] to make the comparisons between T_1, T_2 and T_3, and S_1, S_2 and S_3 fair and maintain the relative order of the similarity scores. In the solid lines are the original normalized values and in the dashed lines the encrypted values.

The visualization illustrates that the optimal matchings, i.e. the highest normalized similarity values, do not change when normalization is applied, namely $T_1 \rightarrow S_2$ with 1.0000, $T_2 \rightarrow S_1$ with 1.0000 and $T_3 \rightarrow S_2$ with 1.0000. This proves that the normalization and the encryption process does not alter the underlying decision structure and ranking of the alternatives, and does not affect the identification of the optimal matches.

In addition, the encryption only causes a small perturbation (±0.0142), which leads to slight differences between the original and encrypted coordinates yet does not significantly affect the trends. This has shown that the proposed privacy-preserving framework is able to preserve the similarity information without being too sensitive, while preserving high accuracy in the analysis and strong data privacy for secure similarity analysis and decision-support applications.

The results are shown in 3D encrypted t-SNE visualization (Figure 3), which indicates that t-SNE process is effective to map the original cotangent similarity coordinates into 3D space in the same way of their overall spatial relationships. The original point (circle) is mapped to the encrypted point (square), and

Table 1. Matrix of target intelligence features based on cotangent similarity ($T \times S$) [80]

	S_1	S_2	...	S_n
T_1	T_{11}, I_{11}, F_{11}	T_{12}, I_{12}, F_{12}	...	T_{1n}, I_{1n}, F_{1n}
T_2	T_{21}, I_{21}, F_{21}	T_{22}, I_{22}, F_{22}	...	T_{2n}, I_{2n}, F_{2n}
...	...	...	...	...
T_m	T_{m1}, I_{m1}, F_{m1}	T_{m2}, I_{m2}, F_{m2}	...	T_{mn}, I_{mn}, F_{mn}

Table 2. Operational classification matrix for target surveillance data ($T \times S \rightarrow C$) [80]

Row-I	S_1	S_2	S_3	Row-II	C_1	C_2	C_3
T_1	$\begin{pmatrix}0.5e^{\iota\pi(0.6)}\\0.7e^{\iota\pi(0.5)}\\0.3e^{\iota\pi(0.3)}\end{pmatrix}$	$\begin{pmatrix}0.6e^{\iota\pi(0.7)}\\0.4e^{\iota\pi(0.4)}\\0.3e^{\iota\pi(0.4)}\end{pmatrix}$	$\begin{pmatrix}0.3e^{\iota\pi(0.2)}\\0.5e^{\iota\pi(0.5)}\\0.8e^{\iota\pi(0.3)}\end{pmatrix}$	S_1	$\begin{pmatrix}0.3e^{\iota\pi(0.4)}\\0.5e^{\iota\pi(0.7)}\\0.7e^{\iota\pi(0.7)}\end{pmatrix}$	$\begin{pmatrix}0.7e^{\iota\pi(0.6)}\\0.6e^{\iota\pi(0.5)}\\0.2e^{\iota\pi(0.3)}\end{pmatrix}$	$\begin{pmatrix}0.5e^{\iota\pi(0.8)}\\0.4e^{\iota\pi(0.7)}\\0.9e^{\iota\pi(0.3)}\end{pmatrix}$
T_2	$\begin{pmatrix}0.4e^{\iota\pi(0.6)}\\0.7e^{\iota\pi(0.9)}\\0.5e^{\iota\pi(0.7)}\end{pmatrix}$	$\begin{pmatrix}0.2e^{\iota\pi(0.4)}\\0.4e^{\iota\pi(0.9)}\\0.6e^{\iota\pi(0.3)}\end{pmatrix}$	$\begin{pmatrix}0.7e^{\iota\pi(0.7)}\\0.4e^{\iota\pi(0.3)}\\0.6e^{\iota\pi(0.6)}\end{pmatrix}$	S_2	$\begin{pmatrix}0.2e^{\iota\pi(0.5)}\\0.3e^{\iota\pi(0.2)}\\0.7e^{\iota\pi(0.3)}\end{pmatrix}$	$\begin{pmatrix}0.6e^{\iota\pi(0.6)}\\0.7e^{\iota\pi(0.8)}\\0.4e^{\iota\pi(0.3)}\end{pmatrix}$	$\begin{pmatrix}0.3e^{\iota\pi(0.6)}\\0.6e^{\iota\pi(0.7)}\\0.8e^{\iota\pi(0.9)}\end{pmatrix}$
T_3	$\begin{pmatrix}0.7e^{\iota\pi(0.9)}\\0.6e^{\iota\pi(0.5)}\\0.8e^{\iota\pi(0.8)}\end{pmatrix}$	$\begin{pmatrix}0.2e^{\iota\pi(0.4)}\\0.8e^{\iota\pi(0.5)}\\0.7e^{\iota\pi(0.6)}\end{pmatrix}$	$\begin{pmatrix}0.6e^{\iota\pi(0.9)}\\0.3e^{\iota\pi(0.6)}\\0.2e^{\iota\pi(0.3)}\end{pmatrix}$	S_3	$\begin{pmatrix}0.4e^{\iota\pi(0.4)}\\0.7e^{\iota\pi(0.5)}\\0.5e^{\iota\pi(0.9)}\end{pmatrix}$	$\begin{pmatrix}0.6e^{\iota\pi(0.2)}\\0.3e^{\iota\pi(0.5)}\\0.4e^{\iota\pi(0.4)}\end{pmatrix}$	$\begin{pmatrix}0.7e^{\iota\pi(0.2)}\\0.3e^{\iota\pi(0.8)}\\0.2e^{\iota\pi(0.3)}\end{pmatrix}$

Table 3. Cotangent similarity scores between signal samples ($S_1 - S_3$) and class templates ($T_1 - T_3$) [80]

Cot SM	S_1	S_2	S_3
T_1	0.4913	0.6653	0.5785
T_2	0.5287	0.4937	0.3576
T_3	0.4110	0.4604	0.4221

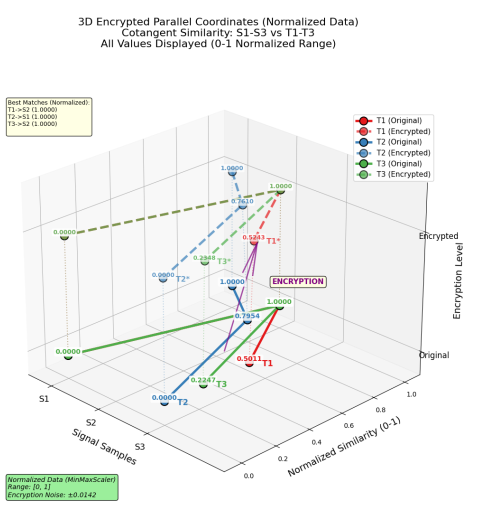

Figure 2. 3D Encrypted Parallel Coordinates (Normalized Data)

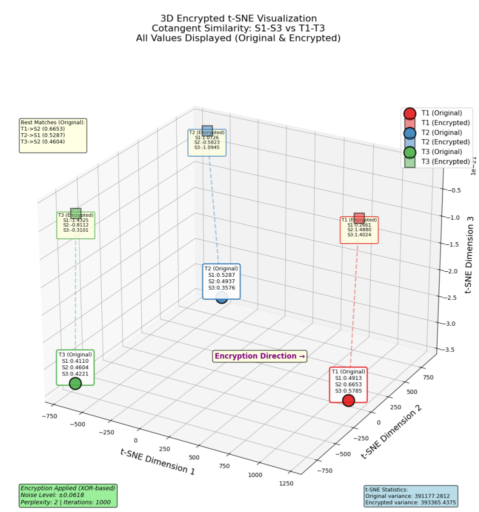

Figure 3. 3D Encrypted t-SNE Visualization

the dashed lines make it easy to see the movement caused by the encryption of the points, but without losing the general order of the samples.

The visualization also reveals that the essential structural properties are preserved after encryption, i.e. T_1, T_2 and T_3 are well-separated, which is necessary for visual analytics. The similarity between the original and encrypted embeddings confirms that the similarity values are only slightly modified to preserve the usefulness of the data for clustering and pattern recognition purposes, while preserving privacy. The overall result shows that the proposed encryption model is effectively used in maintaining both data security and analytical integrity.

The 3D Encrypted Parallel Coordinates (Normalized Data) Figure 4 shows the behavior of the Min-Max normalized similarity values for the cotangent similarity measure, before and after encryption. All similarity scores were rescaled between 0 and 1, so that they can be fairly compared with each other, both between T_1 and T_3, and between S_1 and S_3, maintaining the same relative ordering of the similarity measures. Original normalized values are represented by solid lines, while dashed lines are for the encrypted values.

It can be seen that after normalization the best matching pairs does not change, that is: $T_1 \rightarrow S_2$, $T_2 \rightarrow S_1$ and $T_3 \rightarrow$

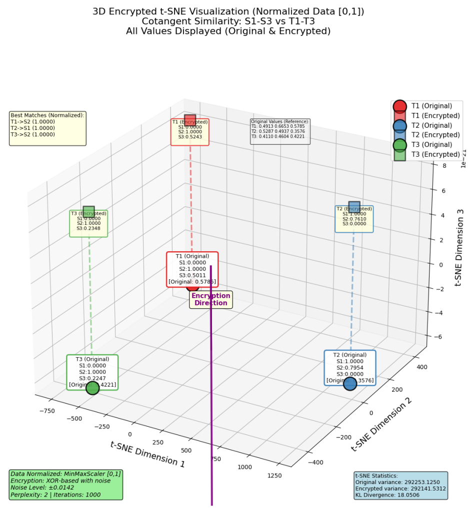

Figure 4. 3D Encrypted Parallel Coordinates (Normalized Data)

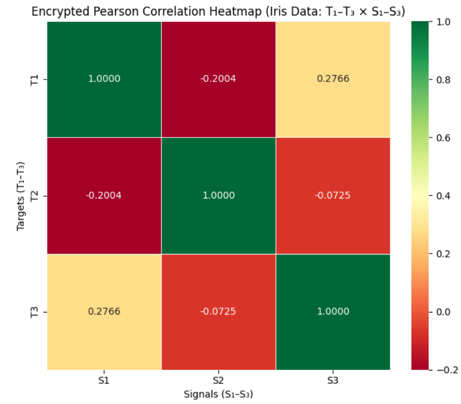

Figure 5. Encrypted Pearson Correlation Heatmap

S_2, all three with the maximum normalized similarity value = 1.0000. This verifies that the decision structure and ranking of the alternatives is retained throughout the normalization and encryption process and that the optimal matches are retained.

In addition, the encryption brings in only a very slight perturbation (±0.0142), with the result that the original coordinates and the encrypted ones differ slightly, but the trends are essentially the same. It shows that the proposed privacy-preserving framework effectively preserves sensitive similarity information with minimum distortion, and maintains high analytical accuracy while providing high data confidentiality for secure similarity analysis and decision-support applications.

The Encrypted Pearson Correlation Matrix of the Iris dataset is represented by the heatmap in Figure 5, which shows the encrypted linear associations between three signals (S_1, S_2, S_3) and three targets (T_1, T_2, T_3). The encrypted Pearson correlation coefficient is represented by each cell; positive values indicate direct correlations, while negative values indicate inverse interactions. Grey tones represent the intermediate values on the color gradient's scale, which ranges from dark red (negative correlation) to dark green (strong positive correlation). As would be predicted for the identical encrypted variables, the diagonal values (1.0000) represent the ideal correlations of oneself. Off-diagonal entries reveal the inter-variable encrypted relationships. In particular:

A weak inverse association is shown by a negative correlation of -0.2004 between T_1 and S_2. T_1 S_3: There is a positive correlation (0.2766) between T_1 and S_3. The correlation between T_2 and S_3 is weakly negative (-0.0725), while the correlation between T_3 and S_1 is moderately positive (0.2766). Overall, the matrix indicates that T_1 and T_3 are more likely to have positive correlations with signal variables, but T_2 has smaller, sometimes negative correlations. This pattern suggests that the relative correlation pattern and variance relationship among the variables are retained despite the data being encrypted. Even if the data is fully encrypted, the Pearson correlation coefficients are computed in a way that maintains relational integrity but not the underlying raw numerical values. Analysts can safely make inferences about relative strength patterns and directional trends (positive or negative). An efficient model for studying inter-variable interactions under encryption is provided by this Encrypted Pearson Correlation Heatmap. It maintains the original values of the underlying dataset while enabling the identification of patterns, relational inferences, and comparison trends.

The Normalized Encrypted Pearson Correlation Matrix of the Iris dataset between three targets (T_1, T_2, T_3) and three signals (S_1, S_2, S_3) following normalization in the 0-1 range is displayed in Figure 6. Each cell displays the normalized encrypted Pearson correlation coefficient; the stronger the encrypted linear correlations, the closer the value is to 1.0000, and the weaker the encrypted linear links, the lower the value. Yellow indicates a medium degree of relationship, whereas the color gradient ranges from red (low correlation) to green (high correlation). The existence of perfect self-correlations of the same encrypted entities is indicated by entries with a diagonal (1.0000). The relationship dynamics between different targets and signals are indicated by off-diagonal values:

There is a partial linear relationship and a moderate (0.3998) encrypted correlation between T_1 and S_2.
The encrypted portions are more aligned, as indicated by the correlation of 0.6383 between T_1 S3. There is a moderately favorable association between T_2 S_3 and T_3 S_1 (0.4637 and 0.6383, respectively). Overall, T_1 and T_3 have greater encrypted associations with the signals than T_2, which has more moderate relationships, according to the normalized correlation structure. The consistency of balanced normalization and preserved encryption across the dataset is indicated by the symmetry along the diagonal.

It is evident that the topology of the correlation is observable even though the data are fully encrypted and normalized. The raw magnitudes are protected by encryption, and all relationships are proportionately scaled by normalization to preserve interpretability. This Normalized Encrypted Pearson Correlation Heatmap provides a very safe display of inter-variable

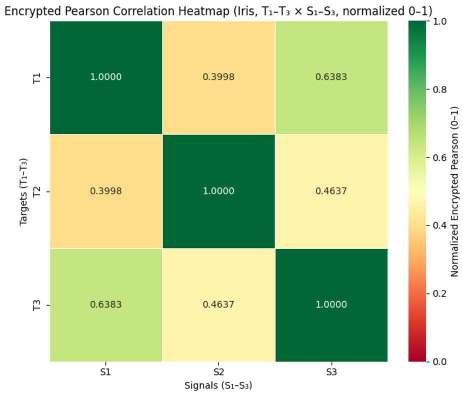

Figure 6. Normalized Encrypted Pearson Correlation Heatmap

connections. It makes it possible to determine the direction and strength of links between encrypted datasets while maintaining analytical validity and interpretability without compromising data privacy or numerical secrecy.

7. Aspect- and method-driven visual structural analysis of encrypted data

An aspect and methodology-based investigation of high-dimensional visual structural analysis of fully encrypted data has been proposed in this paper. Encrypted t-SNE, normalization, parallel coordinates, and encrypted Pearson correlation are used to evaluate data structures without disclosing their original values. Major visual characteristics including class-wise clustering, compactness, and separation are preserved in encrypted 3D embeddings, according to aspect-based research. Method-based analysis demonstrates the stability of neighborhood interactions, dimensional continuity, and correlation patterns with encryption. Experiments on the Iris dataset show that significant structural and visual patterns can be identified while maintaining complete data privacy.

7.1. Aspect-based analysis

The visual and structural characteristics of the encrypted representations offered by different visualization techniques are taken into consideration by the aspect-based analysis. The encrypted and encrypted-plus-normalized 3D t-SNE scatter plots with class-based clustering behavior and privacy requirements are shown in Figures 1 and 2, respectively. Comparative observation of the intra-class compactness and inter-class separation is made possible by the visual coded color encoding in both pictures, which preserves the identity of a class.

While Virginica looks to be more scattered and Versicolor is in midway spaces, the Setosa samples are in a continuous, tighter grouping. Even with full encryption, these patterns remain visible, indicating that the geometrical characteristics of social stratification and local conservation are preserved. This aspect-based observation is transformed into a parallel coordinates space in Figures 3 and 4, where other indicators of the cohesiveness and variety of the classes include the density of the lines, overlap, and dispersion.

Overall, the analysis demonstrates that even if the numbers are normalized and encrypted, important visual characteristics including dispersion patterns, areas of overlap, and clustering propensity can still be understood.

7.2. Method-based analysis

The effectiveness of the used analytical techniques encrypted t-SNE, normalization, parallel coordinates display, and encrypted Pearson correlation analysis is evaluated by the method-based analysis. The 3D t-SNE approach effectively projects high-dimensional encrypted features to a low-dimensional latent space without losing local neighborhood relationships, as seen in Figures 1 and 2.

The even geographical distributions in Figure 2 demonstrate how normalization maximizes comparability among the encrypted dimensions without really changing the underlying relationship structure. Figures 3 and 4 show how analysis based on scatter plots can be supplemented with parallel coordinates plots to display cross-dimensional patterns, continuity, and trends in variances between encrypted samples. Additionally, Figures 5 and 6's encrypted Pearson correlation heatmaps demonstrate how the linear dependency structure is preserved in an encrypted format. The correlation patterns between encrypted and normalized encrypted data validate the analytical pipeline's stability. When combined, these methods enable sophisticated exploratory research without worrying about data confidentiality.

8. Dimensional-based analysis

The distribution and preservation of structural information over decreased dimensions after encryption and normalization are examined by the dimensional-based analysis. 3D scatter plots and parallel coordinates plots illustrate how the three t-SNE dimensions with encryption work together to represent the non-linear relationship in the feature space. Dimensional reduction preserves the neighbors across dimensions since the relative proximity of samples is unaffected by dimensions. While Figures 3 and 4 depict the samples' travel across the tSNE1, tSNE2, and tSNE3 axes, Figures 1 and 2 illustrate that dimensional interaction preserves the relative proximity connections. With Setosa having less variation and Virginica having a wider variance, suggesting the increased complexity within the group, the differentiation in the spread of dimensions shows the varying contributions each latent axis makes to the classification of the classes.

These findings demonstrate the encrypted embeddings' dimensional integrity, enabling significant multi-dimensional analysis without requiring knowledge of the original feature magnitudes.

9. Sensitivity analysis

The stability of structural patterns in the encryption and normalization transformations is assessed using sensitivity analy-

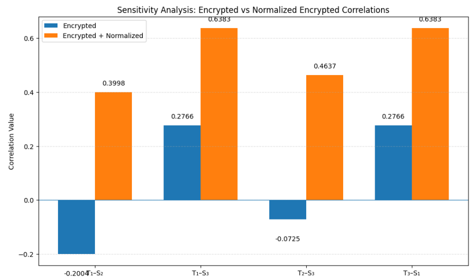

Figure 7. Sensitivity Analysis

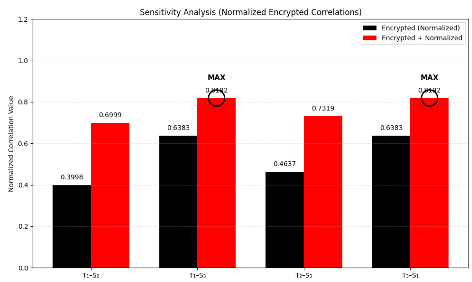

Figure 8. Sensitivity Analysis (Normalized Encrypted Correlation)

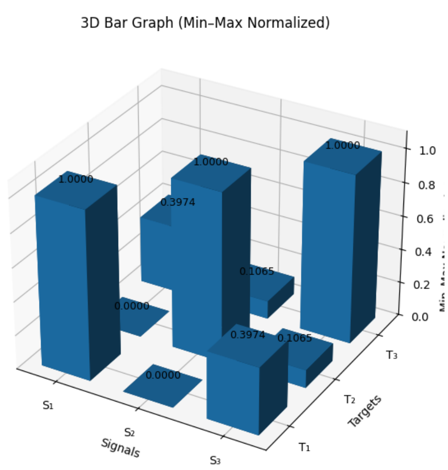

Figure 9. 3D Bar Graph

sis. Figures 1 and 2, as well as Figures 5 and 6, show that normalization merely modifies the magnitude of the relationship, not its topology. Class clustering, dispersion patterns, and correlation hierarchies do not change over time. Controlled sensitivity is demonstrated by small changes in both the correlation strength and the areas of overlap rather than structural degradation. The preservation of dominating correlation pairs that is, greater ties between T_1 and T_3 further demonstrates the capacity to withstand scaling and encryption effects. The research demonstrates that the suggested privacy-preserving architecture guarantees dependable interpretability, protects sensitive data, and is immune to perturbations brought on by transformations.

10. Conclusion

In order to provide a secure high-dimensional data analysis, this work develops a comprehensive model that integrates privacy-sensitive visual analytics with a sophisticated single-valued neutrosophic set theory. A thorough analysis of the fundamental concepts and algebraic properties of CSVNSs confirms their logical consistency and suitability for modeling uncertainty, indeterminacy, and inconsistency. The proposed encrypted visual analytics pipeline demonstrates that the fully encrypted data may be successfully used for correlation analysis, multidimensional visualization, and non-linear dimensionality reduction. Important geometric, topological, and relational features such neighborhood preservation, class-wise dispersion, and inter-variable interdependence are readable even after encryption and normalizing, according to the findings of the experimental application of the Iris dataset. These findings demonstrate the value of CSVNS-based encrypted analytics as a reliable tool for secure exploratory data analysis.

11. Limitations

Regardless of its efficacy, the suggested structure has certain drawbacks. Scalability to very large or streaming datasets has not been thoroughly investigated; the experimental validation was conducted on a benchmark dataset of intermediate size. Despite being an effective visualization method, t-SNE can increase compute overhead and be sensitive to parameter selection, particularly in encrypted environments. Furthermore, the current framework ignores the dynamism of data behavior and more complex dependence measures in favor of fixed datasets and linear correlation analysis. Additionally, the integration of the CSVNS theory with other encryption schemes and privacy models is not the subject of this study.

12. Future work

In the future, there are several methods to expand this framework. More efficient or rudimentary dimensionality reduction algorithms that can handle big encrypted datasets can improve the scalability. The framework can be expanded to handle real-time, dynamic data analysis over encryption. Higher-order correlations, alternative similarity metrics, and neutrosophic-based learning models on encrypted domains would enhance the research's analytical utility. Applying the suggested method to real-world sensitive data in fields like cybersecurity, health care, and finance will further demonstrate its high degree of resistance and practical application.

In addition to intelligent danger detection, further research may explore the novel class of Floquet-engineered point-gapped topological superconductors [81] and non-Hermitian second-order topological phases in photonic kagome crystals [82] with "bipolar" skin effects. By incorporating these cutting-edge concepts into neutrosophic decision making and threat analysis, future generation photonic and defensive technologies, reliable communication systems, quantum sensing, and creative and potent signal processing might all be created.

Data availability

The dataset used in this study is available upon request to the corresponding author.

Declaration of competing interest

The authors declare that they have no competing interests.

Acknowledgment

The authors also extend their appreciation to the Deanship of Scientific Research at Northern Border University, Arar, KSA Saudi Arabia, for supporting this research work through the project number NBU-FFR-2026-2230-04.

References

[1] L. A. Zadeh, "Fuzzy sets", Information and Control **8** (1965) 338. https://doi.org/10.1016/S0019-9958(65)90241-X.
[2] S. S. L. Chang & L. A. Zadeh, "On fuzzy mapping and control", IEEE Transactions on Systems, Man, and Cybernetics **2** (1972) 30. https://doi.org/10.1109/TSMC.1972.5408553.
[3] D. Dubois & H. Prade, "Operations on fuzzy numbers", International Journal of Systems Science **9** (1978) 613. https://doi.org/10.1080/00207727808941724.
[4] K. T. Atanassov, "Intuitionistic fuzzy sets", Fuzzy Sets and Systems **20** (1986) 87. https://doi.org/10.1016/S0165-0114(86)80034-3.
[5] F. Smarandache, *A Unifying Field in Logics Neutrosophy: Neutrosophic Probability*, American Research Press, Rehoboth, DE, USA, 1998. https://doi.org/10.5281/zenodo.49174.
[6] F. Smarandache, "Neutrosophic set, a generalization of the intuitionistic fuzzy sets", International Journal of Pure and Applied Mathematics **24** (2005) 287. https://ijpam.eu/contents/2005-24-3/1/1.pdf.
[7] A. Chakraborty, S. P. Mondal, A. Ahmadian, N. Senu, S. Alam & S. Salahshour, "Different forms of triangular Neutrosophic numbers, De-Neutrosophication techniques, and their applications", Symmetry **10** (2018) 327. https://doi.org/10.3390/sym10080327.
[8] M. Abdel-Basset, A. Atef & F. Smarandache, "A hybrid neutrosophic multiple criteria group decision making approach for project selection", Cognitive Systems Research **57** (2019) 216. https://doi.org/10.1016/j.cogsys.2018.10.023.
[9] L. D. Ojo, O. Adeniyi, O. E. Ogundimu & O. O. Alaba, "Rethinking green supply chain management practices impact on company performance: A close-up insight", Sustainability **14** (2022) 13197. https://doi.org/10.3390/su142013197.
[10] M. Abdel-Baset, V. Chang, A. Gamal & F. Smarandache, "An integrated neutrosophic ANP and VIKOR method for achieving sustainable supplier selection: A case study in importing field", Computers in Industry **106** (2019) 94. https://doi.org/10.1016/j.compind.2018.12.017.
[11] M. Abdel-Basset, M. Ali & A. Atef, "Resource levelling problem in construction projects under neutrosophic environment", Journal of Supercomputing **76** (2019) 964. https://doi.org/10.1007/s11227-019-03055-6.
[12] M. Abdel-Basset, M. Saleh, A. Gamal & F. Smarandache, "An approach of TOPSIS technique for developing supplier selection with group decision making under type-2 neutrosophic number", Applied Soft Computing **77** (2019) 438. https://doi.org/10.1016/j.asoc.2019.01.035.
[13] M. Abdel-Basset, A. Gamal, L. H. Son & F. Smarandache, "A bipolar neutrosophic multi-criteria decision making framework for professional selection", Applied Intelligence **51** (2021) 1.
[14] M. Saqlain, M. N. Jafar & M. Riaz, "A new approach of neutrosophic soft set with generalized fuzzy TOPSIS in application of smart phone selection", Neutrosophic Sets and Systems **32** (2020) 307. https://doi.org/10.5281/zenodo.3723161.
[15] M. Riaz & H. M. A. Farid, "Enhancing green supply chain efficiency through linear Diophantine fuzzy soft-max aggregation operators", Journal of Industrial Intelligence **1** (2023) 8. https://doi.org/10.56578/jii010102.
[16] M. Abdel-Basset & R. Mohamed, "A novel plithogenic TOPSIS-CRITIC model for sustainable supply chain risk management", Journal of Cleaner Production **247** (2020) 119586. https://doi.org/10.1016/j.jclepro.2019.119586.
[17] F. Smarandache, "Neutrosophic logic and set, m-version", Neutrosophic Sets and Systems **55** (2023) 1.
[18] E. K. Zavadskas, A. Mardani, Z. Turskis, A. Jusoh & K. M. Nor, "Development of TOPSIS method to solve complicated decision-making problems: An overview on developments from 2000 to 2015", International Journal of Information Technology Decision Making **15** (2016) 645. https://doi.org/10.1142/S0219622016300019.
[19] H. Garg & K. Kumar, "An advanced study on the similarity measures of intuitionistic fuzzy sets based on the set pair analysis theory and their application in decision making", Soft Computing **22** (2018) 4959. https://doi.org/10.1007/s00500-018-3202-1.
[20] X. Peng & J. Dai, "Research on the assessment of classroom teaching quality with q-rung orthopair fuzzy information based on multiparametric similarity measure and combinative distance-based assessment", International Journal of Intelligent Systems **34** (2019) 1588. https://doi.org/10.1002/int.22109.
[21] M. Akram, W. A. Dudek & J. M. Dar, "Pythagorean Dombi fuzzy aggregation operators with application in multicriteria decision-making", International Journal of Intelligent Systems **34** (2019) 3000. https://doi.org/10.1002/int.22183.
[22] H. Delfs & H. Knebl, *Introduction to Cryptography: Principles and Applications*, Springer, Berlin/Heidelberg, Germany, 2007.
[23] J. Daemen & V. Rijmen, *The Design of Rijndael: AES The Advanced Encryption Standard*, Springer, Berlin/Heidelberg, Germany, 2002. https://doi.org/10.1007/978-3-662-04722-4.
[24] A. Philip, "A generalized pseudo-knight's tour algorithm for encryption of an image", IEEE Potentials **32** (2013) 10. https://doi.org/10.1109/MPOT.2012.2219651.
[25] H. Al-Assam, R. Rashid & S. Jassim, "Combining steganography and biometric cryptosystems for secure mutual authentication and key exchange", Proceedings of the 8th International Conference for Internet Technology and Secured Transactions (ICITST) (2013) 369.
[26] D. Bloisi & L. Iocchi, *Image based steganography and cryptography*, Proceedings of VISAPP, 2007. https://www.researchgate.net/publication/221415424_Image_based_steganography_and_cryptography.
[27] H. Sharma, "Secure image hiding algorithm using cryptography and steganography", IOSR Journal of Computer Engineering **13** (2013) 1.
[28] J. Liu, H. Jin, L. Ma, Y. Li & W. Jin, "Optical color image encryption based on computer generated hologram and chaotic theory", Optics Communications **307** (2013) 76. https://doi.org/10.1016/j.optcom.2013.05.064.
[29] C. E. Shannon, "Communication theory of secrecy systems", Bell System Technical Journal **28** (1949) 656. https://doi.org/10.1002/j.1538-7305.1949.tb00928.x.
[30] D. J. Bachman, E. A. Brown & A. H. Norton, "Chocolate key cryptography", Mathematics Teacher **104** (2010) 100. https://doi.org/10.5951/MT.104.2.0100.
[31] J. Rosenthal, "A polynomial description of the Rijndael advanced encryption standard", Journal of Algebra and Its Applications **2** (2003) 223. https://doi.org/10.1142/S0219498803000532.
[32] C. K. Koc, *Cryptographic Engineering*, Springer, Boston, MA, USA, 2009 pp 125–128.
[33] J. Liu, B. Wei, X. Cheng & X. Wang, *An AES S-box to increase complexity and cryptographic analysis*, Proceedings AINA, 2005. https://doi.org/10.1109/AINA.2005.84.
[34] K. Challita & H. Farhat, "Combining steganography and cryptography: New directions", International Journal of New Computer Architectures and Their Applications **1** (2011) 199.
[35] N. Ferguson, R. Schroeppel & D. Whiting, "A simple algebraic representation of Rijndael", LNCS **2259** (2001) 103. https://doi.org/10.1007/3-540-45537-X-8.
[36] S. Murphy & M. J. B. Robshaw, "Essential algebraic structure within the AES", LNCS **2442** (2002) 1. https://doi.org/10.1007/3-540-45708-9_1.

[37] L. Cui & Y. Cao, "A new S-Box structure named Affine-Power-Affine", International Journal of Innovative Computing, Information and Control **3** (2007) 751.

[38] J. Li, B. Wang & X. Wang, "One AES S-box to increase complexity and its cryptanalysis", Journal of Systems Engineering and Electronics **18** (2007) 427. https://doi.org/10.1016/S1004-4132(07)60108-X.

[39] M. Khan & N. A. Azam, "Right translated AES Gray S-Boxes", Security and Communication Networks **8** (2015) 1627. https://doi.org/10.1002/sec.1110.

[40] M. Khan & N. A. Azam, "S-Boxes based on affine mapping and orbit of power function", 3D Research **6** (2015) 12. https://doi.org/10.1007/s13319-015-0043-x.

[41] M. T. Tran, D. K. Bui & A.-D. Duong, *Gray S-box for advanced encryption standard*, Proceedings CIS, 2008. https://doi.org/10.1109/CIS.2008.205.

[42] F. Smarandache, *A unifying field in logics, neutrosophy: neutrosophic probability, set and logic*, American Research Press, Mexico, 1999. https://fs.unm.edu/eBook-Neutrosophics6.pdf.

[43] A. Ahmad, R. Hatamleh, K. Matarneh & A. Al-Husban, "On the irreversible k-threshold conversion number for some graph products and neutrosophic graphs", International Journal of Neutrosophic Science **25** (2025) 183. https://doi.org/10.54216/IJNS.250216.

[44] A. A. Abubaker, R. Hatamleh, K. Matarneh & A. Al-Husban, "On the numerical solutions for some neutrosophic singular boundary value problems by using (LPM) polynomials", International Journal of Neutrosophic Science **25** (2024) 197. https://doi.org/10.54216/IJNS.250217.

[45] R. Hatamleh & A. Hazaymeh, "On some topological spaces based on symbolic n-plithogenic intervals", International Journal of Neutrosophic Science **25** (2025) 23. https://doi.org/10.54216/IJNS.250102.

[46] R. Hatamleh, A. Al-Husban, K. Sundareswari, G. Balaj & M. Palanikumar, "Complex tangent trigonometric approach applied to (γ, τ)-rung fuzzy set using weighted averaging, geometric operators and its extension", Communications on Applied Nonlinear Analysis **32** (2025) 133. https://doi.org/10.52783/cana.v32.2978.

[47] H. Qawaqneh, "Fractional analytic solutions and fixed point results with some applications", Advances in Fixed Point Theory **14** (2024) 1. https://doi.org/10.28919/afpt/8279.

[48] H. Qawaqneh, M. Noorani, H. Aydi, A. Zraiqat & A. H. Ansari, "On fixed point results in partial b-metric spaces", Journal of Function Spaces **2021** (2021) 8769190. https://doi.org/10.1155/2021/8769190.

[49] H. Qawaqneh, M. S. Noorani & H. Aydi, "Some new characterizations and results for fuzzy contractions in fuzzy b-metric spaces and applications", AIMS Mathematics **8** (2023) 6682. https://doi.org/10.3934/math.2023338.

[50] H. Qawaqneh, J. Manafian, M. Alharthi & Y. Alrashedi, "Stability analysis, modulation instability, and beta-time fractional exact soliton solutions to the van der Waals equation", Mathematics **12** (2024) 2257. https://doi.org/10.3390/math12142257.

[51] H. Qawaqneh, "New functions for fixed point results in metric spaces with some applications", Indian Journal of Mathematics **66** (2024) 55.

[52] H. Qawaqneh, H. A. Hammad & H. Aydi, "Exploring new geometric contraction mappings and their applications in fractional metric spaces", AIMS Mathematics **9** (2024) 521. https://doi.org/10.3934/math.2024028.

[53] R. Hatamleh & A. Hazaymeh, "Finding minimal units in several two-fold fuzzy finite neutrosophic rings", Neutrosophic Sets and Systems **70** (2024) 1. https://doi.org/10.5281/zenodo.13160839.

[54] T. Kanan, M. Elbes, K. Abu Maria & M. Alia, "Exploring the potential of IoT-based learning environments in education", International Journal of Advances in Soft Computing and its Applications **15** (2023) 166. https://doi.org/10.15849/IJASCA.230720.11.

[55] I. M. Batiha, S. A. Njadat, R. M. Batyha, A. Zraiqat, A. Dababneh & S. Momani, "Design fractional-order PID controllers for single-joint robot arm model", International Journal of Advances in Soft Computing and its Applications **14** (2022) 96. https://doi.org/10.15849/IJASCA.220720.07.

[56] A. M. Abd El-latif & M. H. Alqahtani, "Novel categories of supra soft continuous maps via new soft operators", AIMS Mathematics **9** (2024) 7449. https://doi.org/10.3934/math.2024361.

[57] A. M. Abd El-latif, M. H. Alqahtani & F. A. Gharib, "Strictly wider class of soft sets via supra soft d-closure operator", International Journal of Analysis and Applications **22** (2024) 47. https://doi.org/10.28924/2291-8639-22-2024-47.

[58] A. M. Abd El-latif, A. A. Azzam, R. Abu-Gdairi, M. Aldawood & M. H. Alqahtani, "New versions of maps and connected spaces via supra soft sd-operators", PLOS ONE **19** (2024) e0304042. https://doi.org/10.1371/journal.pone.0304042.

[59] A. M. Abd El-latif, A. A. Azzam, R. Abu-Gdairi, M. H. Alqahtani & G. M. Abd-Elhamed, "Applications on soft somewhere dense sets", Journal of Interdisciplinary Mathematics **27** (2024) 1679. https://doi.org/10.47974/JIM-2007.

[60] A. Al-Omari & M. H. Alqahtani, "Some operators in soft primal spaces", AIMS Mathematics **9** (2024) 10756. https://doi.org/10.3934/math.2024525.

[61] M. H. Alqahtani, "Operators and separation axioms within the framework of diving topological spaces", AIMS Mathematics **10** (2025) 25253. https://doi.org/10.3934/math.20251118.

[62] M. H. Alqahtani, "Neutrosophic primal structure with closure and proximity operators", AIMS Mathematics **11** (2026) 644. https://doi.org/10.3934/math.2026028.

[63] M. H. Alqahtani & M. Tkachenko, "Normality and n-factorizable topological groups", Topology and its Applications **373** (2025) 109497. https://doi.org/10.1016/j.topol.2025.109497.

[64] I. Ibedou, S. E. Abbas & M. H. Alqahtani, "Defining new structures on a universal set: Diving structures and floating structures", Mathematics **13** (2025) 1859. https://doi.org/10.3390/math13111859.

[65] S. A. El-Sheikh & A. M. Abd El-latif, "Decompositions of some types of supra soft sets and soft continuity", International Journal of Mathematics Trends and Technology **9** (2014) 37. https://doi.org/10.14445/22315373/IJMTT-V9P504.

[66] A. M. Abd El-latif, "Specific types of Lindelofness and compactness based on novel supra soft operator", AIMS Mathematics **10** (2025) 8144. https://doi.org/10.3934/math.2025374.

[67] A. M. Abd El-latif & M. H. Alqahtani, "New soft operators related to supra soft di-open sets and applications", AIMS Mathematics **9** (2024) 3076. https://doi.org/10.3934/math.2024150.

[68] M. H. Alqahtani & A. M. Abd El-latif, "Separation axioms via novel operators in topological spaces and applications", AIMS Mathematics **9** (2024) 14213. https://doi.org/10.3934/math.2024690.

[69] H. Wang, F. Smarandache, Y. Zhang & R. Sunderraman, "Single valued Neutrosophic sets", in Multispace & Multistructure. Neutrosophic Transdisciplinarity (100 Collected Papers of Sciences), vol. IV, 2010, pp 410–413. Available: https://fs.unm.edu/SingleValuedNeutrosophicSets.pdf.

[70] M. Ali & F. Smarandache, "Complex Neutrosophic set", Neural Computing and Applications **25** (2016) 1. https://doi.org/10.1007/S00521-015-2154-Y.

[71] L. van der Maaten & G. Hinton, "Visualizing data using t-SNE," Journal of Machine Learning Research **9** (2008) 2579. https://doi.org/10.5555/1390681.1390301.

[72] R. Agrawal & R. Srikant, "Privacy-preserving data mining," in Proceedings of the ACM SIGMOD International Conference on Management of Data, 2000, 439. https://doi.org/10.1145/342009.335438.

[73] C. C. Aggarwal & P. S. Yu, *A general survey of privacy-preserving data mining models and algorithms*, in Privacy-Preserving Data Mining: Models and Algorithms, Springer, 2008. https://doi.org/10.1007/978-0-387-70992-5.

[74] J. Han, M. Kamber & J. Pei, *Data Mining: Concepts and Techniques*, 3rd ed., Morgan Kaufmann (2011). https://www.sciencedirect.com/book/9780123814791/data-mining-concepts-and-techniques.

[75] A. Inselberg, "The plane with parallel coordinates", The Visual Computer **1** (1985) 69. https://doi.org/10.1007/BF01898350.

[76] C. Clifton, M. Kantarcioglu & J. Vaidya, "Tools for privacy-preserving distributed data mining," ACM SIGKDD Explorations Newsletter **4** (2002) 28. https://doi.org/10.1145/772862.772867.

[77] K. Pearson, *Notes on regression and inheritance in the case of two parents*, Proceedings of the Royal Society of London, 1895. https://doi.org/10.1098/rspl.1895.0041.

[78] L. Wilkinson, it The grammar of graphics. Springer, 2005. https://doi.org/10.1007/0-387-28695-0.

[79] C. Gentry, *Fully homomorphic encryption using ideal lattices*, in Proceedings of the 41st Annual ACM Symposium on Theory of Computing (STOC), 2009. https://doi.org/10.1145/1536414.1536440.

[80] H. Qawaqneh, W. M. M. Salameh, D. A. M. Mahmoud, G. Nordo, A. Hussain, A. Mehmood & C. L. Armada, "Structure-preserving clustering in

encrypted feature spaces", Statistics, Optimization and Information Computing **16** (2026) 849. https://doi.org/10.19139/soic-2310-5070-3937.
[81] X. Ji, H. Geng, N. Akhtar & X. Yang, "Floquet engineering of Point-Gapped topological superconductors", Physical Review B **111** (2025) 195419. https://doi.org/10.1103/PhysRevB.111.195419.
[82] X. Yang, Y. Feng, A. Wahab & H. Geng, "Non-Hermitian second-order topological phases and bipolar skin effect in photonic Kagome crystals", Physical Review A **113** (2026) 023506. https://doi.org/10.1103/s26b-8bdl.